Cellular/Molecular

The Proteome of BLOC-1 Genetic Defects Identifies the Arp2/3 Actin Polymerization Complex to Function Downstream of the Schizophrenia Susceptibility Factor Dysbindin at the Synapse

Avanti Gokhale,[1]* Cortnie Hartwig,[3,4]* Amanda H. Freeman,[1,2]* Ravi Das,[5]* Stephanie A. Zlatic,[1]* Rachel Vistein,[6]* Amelia Burch,[1] Guillemette Carrot,[4] Arielle F. Lewis,[1] Sheldon Nelms,[3] Dion K. Dickman,[7] Manojkumar A. Puthenveedu,[6] Daniel N. Cox,[5] and Victor Faundez[1]

[1]Department of Cell Biology and [2]Center for the Study of Human Health, Emory University, Atlanta, Georgia 30322, [3]Kennesaw State University, Atlanta, Georgia 30144, [4]Department of Chemistry, Agnes Scott College, Decatur, Georgia 30030, [5]Neuroscience Institute, Center for Behavioral Neuroscience, Georgia State University, Atlanta, Georgia 30302, [6]Biological Sciences, Carnegie Mellon University, Pittsburgh, Pennsylvania 15213, and [7]Department of Biology, Neurobiology Section, University of Southern California, Los Angeles, California 90089

Proteome modifications downstream of monogenic or polygenic disorders have the potential to uncover novel molecular mechanisms participating in pathogenesis and/or extragenic modification of phenotypic expression. We tested this idea by determining the proteome sensitive to genetic defects in a locus encoding dysbindin, a protein required for synapse biology and implicated in schizophrenia risk. We applied quantitative mass spectrometry to identify proteins expressed in neuronal cells the abundance of which was altered after downregulation of the schizophrenia susceptibility factor dysbindin (Bloc1s8) or two other dysbindin-interacting polypeptides, which assemble into the octameric biogenesis of lysosome-related organelles complex 1 (BLOC-1). We found 491 proteins sensitive to dysbindin and BLOC-1 loss of function. Gene ontology of these 491 proteins singled out the actin cytoskeleton and the actin polymerization factor, the Arp2/3 complex, as top statistical molecular pathways contained within the BLOC-1-sensitive proteome. Subunits of the Arp2/3 complex were downregulated by BLOC-1 loss of function, thus affecting actin dynamics in early endosomes of BLOC-1-deficient cells. Furthermore, we demonstrated that Arp2/3, dysbindin, and subunits of the BLOC-1 complex biochemically and genetically interact, modulating *Drosophila melanogaster* synapse morphology and homeostatic synaptic plasticity. Our results indicate that ontologically prioritized proteomics identifies novel pathways that modify synaptic phenotypes associated with neurodevelopmental disorder gene defects.

Key words: Arp2/3; BLOC-1; dysbindin; proteomics; schizophrenia; synapse

Significance Statement

The mechanisms associated with schizophrenia are mostly unknown despite the increasing number of genetic loci identified that increase disease risk. We present an experimental strategy that impartially and comprehensively interrogates the proteome of neurons to identify effects of genetic mutations in a schizophrenia risk factor, dysbindin. We find that the expression of the actin polymerization complex Arp2/3 is reduced in dysbindin-deficient cells, thus affecting actin-dependent phenotypes in two cellular compartments where dysbindin resides, endosomes and presynapses. Our studies indicate that a central cellular structure affected by schizophrenia susceptibility loci is the actin cytoskeleton, an organelle necessary for synaptic function in the presynaptic and postsynaptic compartment.

Introduction

Genomes of individuals affected by polygenic disorders of high hereditability have offered a fertile ground for harvesting risk genes converging into putative disorder mechanisms. Such is the case of schizophrenia, a complex polygenic disorder in which high-confidence genetic risk factors have recently converged into

Received April 21, 2016; revised Oct. 1, 2016; accepted Oct. 20, 2016.

Author contributions: A.G., C.H., A.H.F., R.D., S.A.Z., R.V., A.B., M.A.P., D.N.C., and V.F. designed research; A.G., C.H., A.H.F., R.D., S.A.Z., R.V., A.B., G.C., A.F.L., S.N., and V.F. performed research; D.K.D. contributed unpublished reagents/analytic tools; A.G., C.H., A.H.F., S.A.Z., R.V., D.K.D., M.A.P., D.N.C., and V.F. analyzed data; A.G., R.D., M.A.P., D.N.C., and V.F. wrote the paper.

This work was supported by the National Institutes of Health (Grant GM077569 to V.F. Grants NS086082 and MH086928 to D.N.C.) and Children's Healthcare of Atlanta Children's Center for Neuroscience (V.F.). S.A.Z. was

discrete cellular and molecular pathways (Gilman et al., 2012; Fromer et al., 2014; Purcell et al., 2014). These ontologically informed pathways often implicate synapse function as a pathogenesis mechanism. Individual genetic risk loci are likely to influence the expression of multiple proteins encoded by genes other than the affected locus (Picotti et al., 2013; Wu et al., 2013; Albert et al., 2014). These proteins downstream of a single risk allele could map within a protein complex, cellular pathway, or organelle. This suggests, that in in addition to genomes, proteomes could either widen the spectrum of mechanisms downstream of defined schizophrenia genetic risk factors and/or increase the confidence in putative disorder pathways solely defined by genomic data (Mullin et al., 2013). We hypothesized that proteome modifications downstream of a single gene defect should reveal novel and overlapping mechanisms with pathways defined by genomic studies in schizophrenia patients. We reasoned that this hypothesis could be best examined by studying the proteome sensitive to a gene encoding a subunit of a protein complex that is required for synapse biology and implicated in schizophrenia risk.

We tested this hypothesis using monogenic defects affecting subunits of biogenesis of lysosome-related organelles complex 1 (BLOC-1) (Ghiani and Dell'Angelica, 2011; Gokhale et al., 2012; Mullin et al., 2013). The BLOC-1 complex is an obligate octamer constituted by blos1, 2, 3 (Bloc1s1–3), cappuccino (Bloc1s4), muted (Bloc1s5), pallidin (Bloc1s6), snapin (Bloc1s7), and dysbindin (Bloc1s8) (Ghiani and Dell'Angelica, 2011; Gokhale et al., 2012; Mullin et al., 2013). Importantly, the stability of the BLOC-1 complex strictly requires the integrity of all of its subunits as determined from genetic defects in one subunit, which decrease the expression of transcripts and polypeptides encoding other subunits within the BLOC-1 complex (Huang et al., 1999; Zhang et al., 2002; Ciciotte et al., 2003; Li et al., 2003; Gwynn et al., 2004; Starcevic and Dell'Angelica, 2004; Wei, 2006; Yang et al., 2012; Larimore et al., 2014).

Dysbindin and BLOC-1 subunits localized to the synapse and are required for diverse presynaptic and postsynaptic mechanisms ranging from synaptic vesicle recycling to homeostatic synaptic plasticity (Dickman and Davis, 2009; Newell-Litwa et al., 2009; Newell-Litwa et al., 2010; Larimore et al., 2011; Dickman et al., 2012; Di Giovanni and Sheng, 2015; Gokhale et al., 2015b; Mullin et al., 2015). Predictably, *Bloc1s8* deficiency alleles, such as the *sandy* mouse (*Bloc1s8*$^{sdy/sdy}$) or the *Drosophila dysb*^{1} allele, cause behavioral and cognitive phenotypes, some resembling schizophrenia phenotypes (Cox et al., 2009; Jentsch et al., 2009; Shao et al., 2011; Wolf et al., 2011; Papaleo et al., 2012; Mullin et al., 2015). A powerful argument for a role of the BLOC-1 complex in schizophrenia mechanisms is the observation that dysbindin expression is selectively reduced in the majority of schizophrenia brains regardless of the *DTNBP1* allele encoding dysbindin in these patients (Talbot et al., 2004; Tang et al., 2009; Talbot et al., 2011). Polymorphisms in the gene encoding dysbindin were initially reported as risk factors for schizophrenia, yet this assertion has been challenged by recent genomic meta-analyses (Straub et al., 2002; Gornick et al., 2005; Talbot et al., 2009; Fatjó-Vilas et al., 2011; Mullin et al., 2011; Farrell et al., 2015). This evidence indicates that risk loci outside of the *DTNBP1* locus regulate the expression of dysbindin in individuals affected by schizophrenia and suggests that altered dysbindin protein expression is a better disorder risk predictor.

Here, we used quantitative mass spectrometry to identify proteins with expression that is modified by diminishing the expression of one of three BLOC-1 subunits, muted (Bloc1s5), pallidin (Bloc1s6), and dysbindin (Bloc1s8), in neuronal cells. We defined 491 proteins sensitive to dysbindin and BLOC-1 loss of function, the BLOC-1-sensitive proteome, which we prioritized statistically by gene ontology (GO) analyses. Unbiased GO brought into focus the actin polymerization factor, the Arp2/3 complex. Conditional genetic disruption of the Arp2/3 complex causes schizophrenia endophenotypes in mouse (Kim et al., 2015). Furthermore, Arp2/3 subunit transcripts are decreased in the prefrontal cortex of schizophrenia patients, revealing the relevance of the Arp2/3 complex for the pathogenesis of schizophrenia (Datta et al., 2016). We demonstrated that Arp2/3 interacts genetically with dysbindin and the BLOC-1 complex subunits Blos1 and pallidin to modulate *Drosophila* neuromuscular synapse morphology and homeostatic synaptic plasticity, an adaptive response of the presynaptic compartment (Dickman and Davis, 2009; Dickman et al., 2012; Gokhale et al., 2015b). As predicted, the proteome sensitive to BLOC-1 deficiencies enriched gene products implicated in psychosis and schizophrenia risk and GO categories previously associated with schizophrenia gene candidates identified in population genomic studies. Our results indicate that ontologically prioritized proteomics identify novel synaptic mechanisms downstream of individual neurodevelopmental disorder risk factors. We propose that protein expression traits emanating from disorder risk alleles expand and strengthen mechanistic insight gained from population genomic studies.

Materials and Methods

Animals. We used C57BL/6 and *Bloc1s8*$^{sdy/sdy}$ mice (*Mus musculus*) described previously. Animals of both sexes were used (Larimore et al., 2014). Animal procedures and studies were approved by the Emory University Institutional Animal Care and Use Committee.

Antibodies. Antibodies against rabbit ArpC2 and ArpC5 (15058-1-AP and 16717-1-AP, 1:1000 blot dilution; ProteinTech Group), rabbit ArpC2 used for immunoprecipitation (07-227, 1 μg; Millipore), rabbit plexin A2 (6896, 1:1000 blot dilution; Cell Signaling Technology), rabbit dysbindin (HPA029616, 1:125 blot dilution; Sigma-Aldrich), rabbit ataxin 2 (A301-118A, 1:2000 blot dilution; Bethyl), mouse VAMP7 (1:750 blot dilution; a gift from Dr. A.A. Peden, Sheffield University, UK), mouse pallidin clone 2G6 (1:500 blot dilution; a gift from Dr. Esteban Dell'Angelica, University of California–Los Angeles), rabbit FAM21 (MC2188, 1:2000 blot dilution; a gift from Dr. Daniel Billadeau, Mayo Cilinic, Rochester, MN), rabbit strumpellin (SC87442, 1:1000 blot dilution; Santa Cruz Biotechnology), mouse actin clone AC-15 (A5451, 1:500 blot dilution; Sigma-Aldrich) mouse monoclonal SV2 (Clone 10H, 1:500 blot dilution; Developmental Studies Hybridoma Bank), mouse monoclonal HSP90 (610418, blot dilution 1:1000; BD Biosciences), and mouse monoclonal FLAG (M2 clone, F-3165, 1 μg used for immunoprecipitation, blot dilution 1:1000; Sigma-Aldrich).

Cell culture, homogenate preparation, and brain fractionation. HEK293T and SH-SY5Y cells (American Type Culture Collection), WASH$^{flox/flox}$, and WASH-null mouse embryonic fibroblasts were cultured in DMEM supplemented with 10% fetal bovine serum (FBS) and 100 μg/ml penicillin and streptomycin (Hyclone) at 37°C in 10% CO_2. *Bloc1s5*$^{mu/mu}$, *Bloc1s6*$^{pa/pa}$, and rescued melanocytes were a gift from

supported by the National Institute of Environmental Health Sciences–National Institutes of Health (T32 Graduate and Postdoctoral Training in Toxicology Training Grant 1P50NS071669). The Emory University Integrated Cellular Imaging Microscopy Core and Viral Cores of the Emory Neuroscience is supported by National Institute of Neurological Disorders and Stroke–National Institutes of Health Core Facilities Grant P30NS055077. We thank members of the Faundez laboratory for comments on the manuscript and Maria Olga Gonzalez Gonzalez for support during the manuscript revision process.

The authors declare no competing financial interests.

*A.G., C.H., A.H.F., R.D., S.A.Z., and R.V. contributed equally to this work.

Correspondence should be addressed to either Avanti Gokhale or Victor Faundez, Department of Cell Biology, Emory University, Atlanta, GA 30322. E-mail: agokhal@emory.edu or vfaunde@emory.edu.

DOI:10.1523/JNEUROSCI.1321-16.2016

 0270-6474/16/3612394-19$15.00/0

Dr. Michael Marks (Department of Pathology and Laboratory Medicine, University of Pennsylvania, Philadelphia; Setty et al., 2007; Setty et al., 2008). WASH $^{flox/flox}$ and WASH-null mouse embryonic fibroblasts were gifts from Dr. Daniel Billadeau (Department Medical Oncology, College of Medicine, Mayo Clinic, Rochester, MN; Gomez et al., 2012). MNT-1 cells were a generous gift from Dr. Vincent Hearing and were cultured as described previously (Kushimoto et al., 2001). shRNA-mediated Bloc1s5 muted and Bloc1s6 pallidin knockdowns were generated as described previously (Gokhale et al., 2015b). Briefly, shRNA in a pLKO.1 vector for lentiviral infection was obtained from Open Biosystems (Pallidin, Clone ID: TRCN0000122781; Muted, Clone ID: TRCN0000128812). Control shRNA in pLKO.1 was obtained from Addgene (vector 1864). For shRNA-mediated dysbindin knockdowns, shRNA in a psiHIV-U6 vector for lentiviral infection was obtained from GeneCopoeia (Dysbindin, catalog #HSH020444-1HIVU6). Control shRNA in a psiHIV-U6 vector was also obtained from GeneCopoeia (control, catalog #CSCHCTR001-HIVU6). SH-SY5Y cells were treated with lentiviral particles for 7 d to obtain efficient knockdown. After day 3 of lentiviral infection, cells were maintained in DMEM supplemented with 10% FBS and selected with puromycin (2 μg/ml; Invitrogen). Detergent-soluble cellular lysates were prepared as described previously (Gokhale et al., 2015b). Briefly, cells were scraped from the dish and cell homogenates were centrifuged at 16,100 $\times$ *g* for 10 min. The clarified supernatant was recovered and measured for total protein content. Samples were resolved by SDS-PAGE and contents were analyzed by immunoblot as described previously (Gokhale et al., 2015b).

Adult brains (postnatal day 50, P50) of C57BL/6 and *Bloc1s8* $^{sdy/sdy}$ mice were fractionated according to the Nagy and Delgado-Escueta (1984) method except that we used the P2 fractions as a crude synaptosome preparation for immunoblot analysis. A total of six animals were fractionated in three independent experiments.

Stable isotope labeling by amino acids in cell culture (SILAC) quantitative mass spectrometry. SH-SY5Y cells were labeled using the protocol described previously by us (Perez-Cornejo et al., 2012; Ryder et al., 2013; Gokhale et al., 2015b). Briefly, cells were grown in DMEM with either "light" unlabeled arginine and lysine amino acids (R0K0) or "heavy" ^{13}C- and ^{15}N-labeled arginine and ^{13}C- and ^{15}N-labeled lysine amino acids (R10K8) supplemented with 10% FBS and 100 μg/ml penicillin and streptomycin and, in some cases, 2 μg/ml puromycin. Cells were grown for a minimum of seven passages, ensuring incorporation of the amino acids in the cellular protein pool at >98%. All reagents for SILAC labeling were obtained from Dundee Cell Products. Cell lysates were prepared as described below and analyzed by mass spectrometry, as described previously (Perez-Cornejo et al., 2012; Ryder et al., 2013; Gokhale et al., 2015b). SILAC mass spectrometry services were contracted from MSBioworks (http://www.msbioworks.com/)

Tandem mass tagging (TMT) quantitative mass spectrometry. Whole brain tissue from C57BL/6 and *Bloc1s8* $^{sdy/sdy}$ P1 mice was flash frozen in liquid nitrogen and stored at −80°C. Tissue was homogenized in 500 μl of urea lysis buffer (8 M urea, 100 mM NaH_2PO_4, pH 8.5), including 5 μl of (100× stock) HALT protease and phosphatase inhibitor mixture (Pierce). Homogenization was performed using a Bullet Blender (Next Advance) according to the manufacturer's protocols. Briefly, each tissue piece was added to urea lysis buffer in a 1.5 ml Rino tube (Next Advance) harboring 750 mg stainless steel beads (0.9–2 mm in diameter) and blended twice for 5 min intervals in the cold room (4°C). Protein supernatants were transferred to 1.5 ml Eppendorf tubes and sonicated (Sonic Dismembrator; Fisher Scientific) 3 times for 5 s with 15 s intervals of rest at 30% amplitude to disrupt nucleic acids and subsequently vortexed. Protein concentration was determined by the bicinchoninic acid method and samples were frozen in aliquots at −80°C. Protein homogenates (100 μg) were diluted with 50 mM triethylammonium bicarbonate (TEAB) to a final concentration of <2 M urea and then treated with 1 mM dithiothreitol at 25°C for 30 min, followed by 5 mM iodoacetimide at 25°C for 30 min in the dark. Protein was digested with 1:100 (w/w) lysyl endopeptidase (Wako) at 25°C for 2 h and further digested overnight with 1:50 (w/w) trypsin (Promega) at 25°C. Resulting peptides were desalted with a Sep-Pak C18 column (Waters). An aliquot equivalent to 20 μg of total protein was taken out of each sample and combined to obtain a global internal standard (GIS) use later for TMT labeling (the total was split into eight aliquots equivalent to 70 μg of total protein). An additional aliquot of 10 μg was taken from each sample to test the digestion efficiency and overall peptide composition. Samples were dried down using a Savant SpeedVac (ThermoFisher Scientific).

TMT labeling was performed according to the manufacturer's protocol. Briefly, the reagents were allowed to equilibrate to room temperature. Dried peptide samples (70 μg each) were resuspended in 100 μl of 100 mM TEAB buffer (supplied with the kit). Anhydrous acetonitrile (41 μl) was added to each labeling reagent tube and the peptide solutions were transferred into their respective channel tubes. The reaction was incubated for 1 h and quenched for 15 min afterward with 8 μl of 5% hydroxylamine. All samples were combined and dried down. Peptides were resuspended in 100 μl of 90% acetonitrile and 0.01% acetic acid. The entire sample was loaded onto an offline electrostatic repulsion–hydrophilic interaction chromatography fractionation HPLC system and 40 fractions were collected over a time of 40 min. The fractions were combined into 20 and dried down. Dried peptide fractions were resuspended in 30 μl of peptide loading buffer (0.1% formic acid, 0.03% trifluoroacetic acid, 1% acetonitrile). Peptide mixtures (2 μl) were separated on a self-packed C18 (1.9 μm Dr. Maisch, Germany) fused silica column (25 cm $\times$ 75 μM internal diameter; New Objective) by a Dionex Ultimate 3000 RSLCNano and monitored on a Fusion mass spectrometer (ThermoFisher Scientific). Elution was performed over a 140 min gradient at a rate of 300 nl/min with buffer B ranging from 3% to 80% (buffer A: 0.1% formic acid in water, buffer B: 0.1% formic in acetonitrile). The mass spectrometer cycle was programmed to collect at the top speed for 3 s cycles in synchronous precursor selection mode. The MS scans (380-1500 *m/z* range, 200,000 AGC, 50 ms maximum ion time) were collected at a resolution of 120,000 at *m/z* 200 in profile mode. CID MS/MS spectra (1.5 *m/z* isolation width, 35% collision energy, 10,000 AGC target, 50 ms maximum ion time) were detected in the ion trap. HCD MS/MS/MS spectra (2 *m/z* isolation width, 65% collision energy, 100,000 AGC target, 120 ms maximum ion time) of the top 10 MS/MS product ions were collected in the Orbitrap at a resolution of 60000. Dynamic exclusion was set to exclude previous sequenced precursor ions for 30 s within a 10 ppm window. Precursor ions with +1 and +8 or higher charge states were excluded from sequencing.

MS/MS spectra were searched against a Uniprot curated mouse database (downloaded on 03/06/2015 with 53289 target sequences) with Proteome Discoverer 2.1 (ThermoFisher Scientific). Methionine oxidation (+15.9949 Da), asparagine, and glutamine deamidation (+0.9840 Da) and protein *N*-terminal acetylation (+42.0106 Da) were variable modifications (up to 3 allowed per peptide); static modifications included cysteine carbamidomethyl (+57.0215 Da), peptide *n* terminus TMT (+229.16293 Da), and lysine TMT (+229.16293 Da). Only fully tryptic peptides were considered with up to two miscleavages in the database search. A precursor mass tolerance of $\pm$20 ppm and a fragment mass tolerance of 0.6 Da were applied. Spectra matches were filtered by Percolator to a peptide-spectrum matches false discovery rate of <1%. Only razor and unique peptides were used for abundance calculations. Ratio of sample over the GIS of normalized channel abundances were used for comparison across all samples.

Microscopy. HEK293T cells stably expressing Signal-Sequence FLAG tagged β-2 adrenergic receptors (SSF-B2AR) were used. Cells were treated with scrambled or Bloc1s6 shRNAs, selected for 7 d in puromycin, and transiently transfected with LifeAct-GFP, LifeAct-RFP, or Actin-GFP. Cells were imaged 10 min after the addition of 10 μM isoproterenol to induce receptor internalization. Functional endosomes were labeled using anti-flag M1 antibody conjugated to Alexa Fluor-647 dye. Cells were grown on coverslips and maintained in 10% FBS (Invitrogen) high-glucose DMEM (HyClone) and imaged in Opti-MEM (Invitrogen) with 10% FBS and buffered to pH 7.4 with 40 mM HEPES. Live-cell confocal images were collected on an Andor Revolution XD Spinning Disk system with a Nikon Eclipse Ti inverted microscope. Objective used for capture was a 100× 1.49 numerical aperture TIRF objective from Nikon. Both microscope and objectives were housed in a temperature-controlled case maintained at 37°C. Light sources were 488 nm and 561 and 647 nm solid-state lasers and images were captured on an iXON + 897 EM-CCD

Camera using Andor iQ. Image analysis was performed on raw images in ImageJ. Images were not modified in anyway other than color and brightness/contrast assignment for multichannel images.

Drosophila *stocks, rearing, genetics, electrophysiology, and microscopy*. All fly stocks (*Drosophila melanogaster*) were reared and maintained at 25°C on two food formulations. All fly experiments were performed on female animals. The food formulation was prepared with 2.7 l of water, 96 g of yeast, 240 g of cornmeal, 18 g of agar, 240 g of molasses, 18 ml of propionic acid, 48 g of tegosep, and 48 ml of ethanol (Mullin et al., 2015). DD food was used as described previously by Dickman et al. (Dickman and Davis, 2009; Dickman et al., 2012) and made as follows: 2.7 l of water, 33 g of yeast, 163 g of cornmeal, 16 g of agar, 200 ml of corn syrup, 4.3 g of tegosept, and 34 ml of ethanol. For crosses, standard second and third chromosome balancers were used. w^{1118} and other fly strains such as balancer chromosome containing $dysb^{1}$ and $blos1^{ex65}$ were described previously (Mullin et al., 2015). $Arpc1^{Q25st/+}$ and $Arpc1^{Q25sd/+}$ were a gift from Dr. Lynn Cooley of Yale University (Hudson and Cooley, 2002). Two additional stocks of w^{1118} animals were obtained from the Bloomington Stock Center (#5905 and #3605). Additional fly strains used in this study included w^{1118},*ppk-EGFP; Sp/CyO* (Grueber et al., 2003); *y,w,hsFLP; Arpc1*^{Q25sd},FRT^{40A} (Bloomington stock #9137); and *w,GAL4*$^{5-40}$,*UAS-Venus.pm,SOP-FLP*^{42};*tubP-GAL80,*FRT^{40A} (Shimono et al., 2014). Live confocal imaging was performed as described previously (Iyer et al., 2013b). Briefly, live third-instar larvae were placed on a microscope slide, immersed in 1:5 (v/v) diethyl ether to halocarbon oil, and covered with a 22 × 50 mm glass coverslip. Neurons expressing GFP were visualized on a Zeiss LSM 780 confocal microscope. Images were collected as *z*-stacks using a 20× dry objective at a step-size of 2.0 μm and 1024 × 1024 resolution. MARCM analyses were performed essentially as described previously (Sulkowski et al., 2011). Briefly, for generating dendritic arborization (DA) neuron MARCM clones, *Arpc1*^{Q25sd},*FRT40A* flies were crossed to *w,GAL4*$^{5-40}$,*UAS-Venus.pm,SOP-FLP*^{42};*tubP-GAL80,*FRT^{40A} flies (DGRC stock #109-947). Third instar larvae with GFP-labeled neurons were subjected to live-cell confocal microscopy. Larval dissections, immunohistochemistry, and confocal microscopy were conducted as described previously (Franciscovich et al., 2008). Wandering third-instar female larvae were dissected in normal HL3, fixed in 4% paraformaldehyde for 1 h, and stained with HRP–FITC for 2 h at room temperature (1:500). An inverted 510 Zeiss LSM microscope was used for confocal imaging of synapses at muscle 6/7 on either the second or third segment. Homeostatic synaptic plasticity studies were performed as described previously (Dickman and Davis, 2009; Dickman et al., 2012; Gokhale et al., 2015b).

Quantitative analyses of neuronal reconstructions were performed as described previously (Iyer et al., 2013a) with some modifications. Maximum-intensity projections of the *z*-stacks were exported as jpeg or tiff files using Zeiss Zen-blue software. Exported images were curated manually to eliminate nonspecific autofluorescent spots such as the larval denticle belts using a custom-designed program, *Flyboys* (Cox Laboratory). The raw pixel intensity for each image was globally thresholded and converted to a binary file format in Photoshop (Adobe). Background image noise was filtered out using the Analyze Particles plugin (http://rsbweb.nih.gov/ij/docs/menus/analyze.html#ap) in ImageJ [size (pixels2) $\leq$50 μm, circularity $\geq$0.35]. Next, images were skeletonized (conversion to 1-pixel-wide "skeletons") using the Skeletonize3D plugin (http://fiji.sc/wiki/index.php/Skeletonize3D) in Fiji/ImageJ followed by use of the Analyze Skeleton Fiji/ImageJ plugin (http://fiji.sc/wiki/index.php/AnalyzeSkeleton) for the output of quantitative neurometric measures of dendritic morphology. Quantitative neurometric information including total dendritic length and total dendritic branches were extracted and compiled using custom Python algorithms and imported into Microsoft Excel. For Strahler analysis, a Fiji plugin (http://fiji.sc/Strahler_Analysis) was used to analyze the skeletonized images by iteratively pruning terminal branches and determining the branch number in each iteration.

The precise deletion of the *pallidin* locus was generated using FLP-mediated recombination between pairs of transposon-based Flp recombinase target (FRT) sites, as described in the DrosDel Collection (Parks et al., 2004). Specifically, two transposons flanking the *pallidin* locus, *PBac{WH}f05716* and *PBac{WH}f05753*, were obtained from the Bloomington *Drosophila* Stock Center. Each contained FRT sites in the correct orientation to permit a precise deletion. After FLP-mediated recombination and excision of the remaining hybrid transposon, we confirmed the deletion by PCR using the following primers: forward primer 5′-TCCCGAGCTGCATGTTGAAT; reverse primer 5′-GTTTGAAACTTAGCTGCGCGA. This revealed that bases 11,689,5565 to 11,691,527 on chromosome 3L were deleted.

Bioinformatics. Gene list to disease associations were performed with the GDA algorithm (http://gda.cs.tufts.edu/; Park et al., 2014) and gene expression analysis was performed with the CSEA tool (http://genetics.wustl.edu/jdlab/csea-tool-2/; Dougherty et al., 2010). Three algorithms were used to perform GO analysis. The BLOC-1-sensitive proteome was analyzed by GeneTerm Linker (http://gtlinker.cnb.csic.es/gtset/index; Fontanillo et al., 2011), ENRICH (http://amp.pharm.mssm.edu/Enrichr/; Chen et al., 2013), and Database Annotation, Visualization and Integrated Discovery (DAVID, https://david.ncifcrf.gov; Huang Da et al., 2009). Cytoscape with Enrichment Map plugin for visualizing DAVID outputs was used to depict integrations between GO terms associated with the BLOC-1-sensitive proteome (Shannon et al., 2003; Merico et al., 2010). Briefly, gene lists uploaded to DAVID were analyzed by setting annotations based by species (*Homo sapiens*) in annotation databases such as GOTERM_BP_FAT or GOTERM_CC_FAT, which would produce a functional annotation chart for molecular function and cellular component, respectively (Huang Da et al., 2009). Parameters for these functional annotation charts included *p*-value cutoff ($<$0.01), a minimum number of three genes for each GO term, fold enrichment, and Bonferroni and/or Benjamini corrected statistical analysis to control for false discovery (Huang Da et al., 2009). Charts were narrowed down to simplify Cytoscape representations by eliminating broad GO terms.

Statistical analysis. Experimental conditions were compared using Synergy Kaleida-Graph version 4.1.3 as specified in each figure.

Results

Identification of a Dysbindin-BLOC-1-sensitive proteome

Deficiencies in dysbindin and other BLOC-1 subunits generate phenotypes in multiple cellular systems, yet a comprehensive understanding of molecular mechanisms upstream or downstream of each one of these phenotypes is still lacking. We sought to answer this question in neuronal tissue because dysbindin is required for synapse function and plasticity and because dysbindin expression is reduced in the majority of schizophrenia brains (Talbot et al., 2004; Mullin et al., 2011; Talbot et al., 2011; Ghiani and Dell'Angelica, 2011). We hypothesized that molecular mechanisms sensitive to dysbindin-BLOC-1 complex deficiencies should be represented as pathway-specific changes in protein expression, should enrich gene products implicated in schizophrenia risk, and should include gene products capable of modifying the phenotypic expression of dysbindin-BLOC-1 mutant alleles.

We began testing this hypothesis and its predictions by quantitatively profiling protein expression in $Bloc1s8^{sdy/sdy}$ mouse brains and human SH-SY5Y neuroblastoma cells in which we downregulated the expression of one BLOC-1 subunit (Fig. 1). The quantitative proteome of mutant and wild-type P0 mouse brains was determined using *in vitro* 10-plex tandem mass tagging of brain homogenate peptides with isobaric tag reagents (TMT; Thompson et al., 2003). We focused on P0 mouse brains because the highest expression of dysbindin occurs during late embryonic development and declines progressively after birth (Ghiani et al., 2010). The quantitative proteome of control and BLOC-1 downregulated neuroblastoma cells was determined by *in vivo* SILAC (Fig. 1; Ong et al., 2002).

We simultaneously quantitated 5922 proteins from four wild-type and five $Bloc1s8^{sdy/sdy}$ mutant brains by TMT and identified 270 proteins with content that was modified significantly by the mutation (Fig. 2*A*,*A2*). Of these proteins, 161 were upregulated and 109 were downregulated in $Bloc1s8^{sdy/sdy}$ brains (Fig. 2*A1*,*A2*). Among the proteins downregulated were just two known proteins with ex-

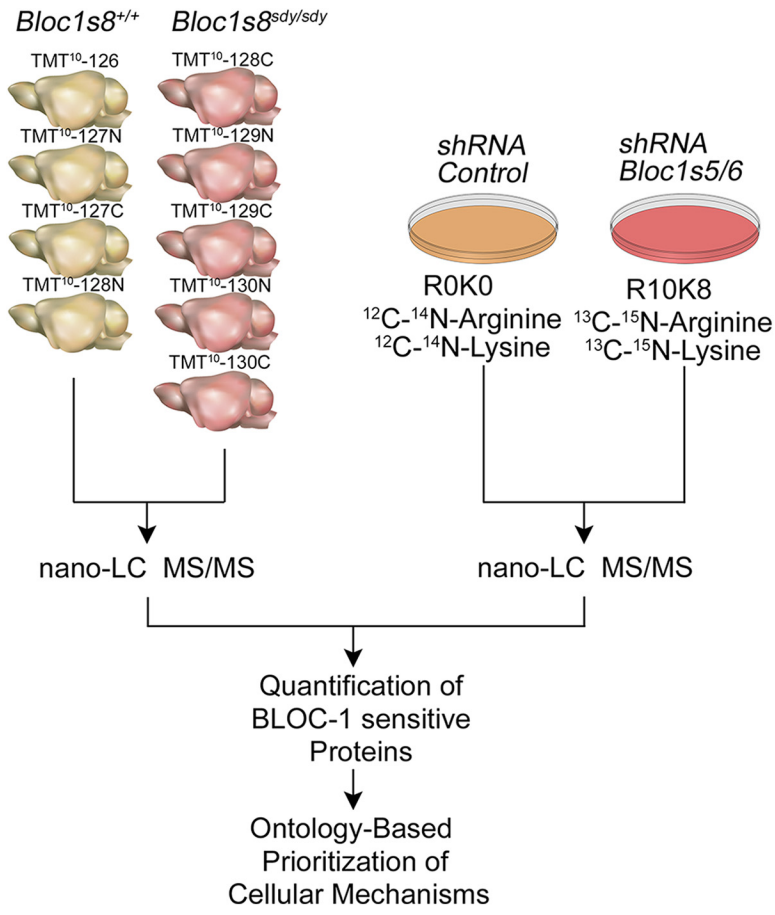

Figure 1. Experimental design to obtain and prioritize the BLOC-1-sensitive proteome. Shown is the experimental work flow to determine the BLOC-1-sensitive proteome using quantitative mass spectrometry to compare the proteomes of wild-type and null dysbindin brains (*Bloc1s8* $^{sdy/sdy}$) by TMT as well as neuroblastoma cells control and rendered deficient in BLOC-1 by shRNA using SILAC.

pression that is reduced in BLOC-1 deficiencies, the BLOC-1 subunit Bloc1s1 and Vamp7 (Fig. 2*A2*; Starcevic and Dell'Angelica, 2004; Salazar et al., 2006; Newell-Litwa et al., 2010). Therefore, the identification of BLOC-1-sensitive proteins might have been compromised by the complexity of whole-brain proteomes. Therefore, we complemented the whole-brain proteome studies with quantitative SILAC proteome analyses of SH-SY5Y neuroblastoma cells (Fig. 1). We reasoned that a homogeneous cell line would allow identification of additional proteins in which a BLOC-1-dependent expression phenotype might be masked by different penetrance because of age, multiplicity of cell types, and anatomical region in brains. Neuroblastoma cells were transduced with lentiviruses expressing a control shRNA or hairpins against the BLOC-1 subunits Bloc1s5 or Bloc1s6. The BLOC-1-targeting hairpins selectively and strongly downregulated the expression of dysbindin (Bloc1s8) in neuroblastoma cells (see Fig. 5*A*). We performed five independent SILAC experiments totaling 16,496 protein quantitations (Fig. 2*B*). SILAC proteomics identified 221 proteins in which the content was selectively modified by downregulation of the BLOC-1 subunits Bloc1s5 or Bloc1s6 (Fig. 2*B*). Upregulated and downregulated proteins were evenly distributed (Fig. 2*B1*,*B2*). We identified the BLOC-1 subunits Bloc1s4 (CNO) and Bloc1s5 (MUTED), the SNARE VAMP7, the copper transporter ATP7A, the *n*-ethymaleimide-sensitive factor, as well as other components of the vesicle fusion apparatus (STXBP1 and 5) and annexin A2 (ANXA2). We reported previously that these molecules are downregulated in BLOC-1 deficiency and participate in common mechanisms with BLOC-1, thus validating our proteome (Newell-Litwa et al., 2010; Gokhale et al., 2015a; Gokhale et al., 2015b; Delevoye et al., 2016). We additionally selected Ataxin 2 and plexin A2 for confirmation because they suggest novel mechanisms intersecting with BLOC-1, including mRNA metabolism and semaphorin receptor activity (Suto et al., 2007; Lim and Allada, 2013; Yokoshi et al., 2014). Ataxin 2 (ATXN2) and plexin A2 (PLXNA2) were upregulated in the proteome, a result that we confirmed in neuroblastoma cells in which BLOC-1 was downregulated by distinct BLOC-1 subunit shRNAs (Fig. 2*B1* and see Fig. 5*A–C*, *A1–C1*). Collectively, TMT and SILAC quantitative mass spectrometry generated a candidate list of 491 proteins sensitive to dysbindin and BLOC-1 loss of function, henceforth referred to as the BLOC-1-sensitive proteome.

The BLOC-1-sensitive proteome significantly enriched gene products implicated in neurodevelopmental disorders such as schizophrenia. This disorder ranked among the three top hits according to the GDA algorithm (Park et al., 2014; Fig. 3*A*). This statistical association of the BLOC-1-sensitive proteome with schizophrenia was further strengthened by its similarity to other gene sets associated with schizophrenia, which are enriched in gene products expressed in human fetal brain development (Gulsuner et al., 2013; Network and Pathway Analysis Subgroup of Psychiatric Genomics, 2015; Fig. 3*B*). Moreover, the BLOC-1-sensitive proteome predicted a significant enrichment of gene products in developing hippocampus, amygdala, and thalamus (Fig. 3*B*). These brain regions are the most compromised by volume reductions in adult schizophrenia patients (van Erp et al., 2016; Okada et al., 2016). These unbiased analyses indicate that the BLOC-1-sensitive proteome enriches gene products and anatomical domains implicated in neurodevelopmental disorders.

Ontological prioritization of BLOC-1 converging pathways

The overlap between the brain and the neuroblastoma BLOC-1-sensitive proteomes was limited to just 12 proteins, suggesting that convergence between these proteomes could occur at a higher organization level such as a pathway, cellular compartment, or protein complex. We used GO bioinformatic tools to test whether the brain and the SH-SY5Y neuroblastoma BLOC-1-sensitive proteomes converge onto known and novel cellular processes (Fig. 4). We sought to prioritize statistically the ontological categories for hypothesis formulation and testing (Fig. 1). We investigated whether GO terms associated just with the proteome identified in SH-SY5Y neuroblastoma cells would be any different from the ontology terms derived from the mouse sensitive proteome and the BLOC-1-sensitive proteome, which encompasses both the SH-SY5Y neuroblastoma and mouse brain proteomes. We used the GeneTerm Linker tool, which relies on fuzzy linkage between genes and ontology terms to identify their

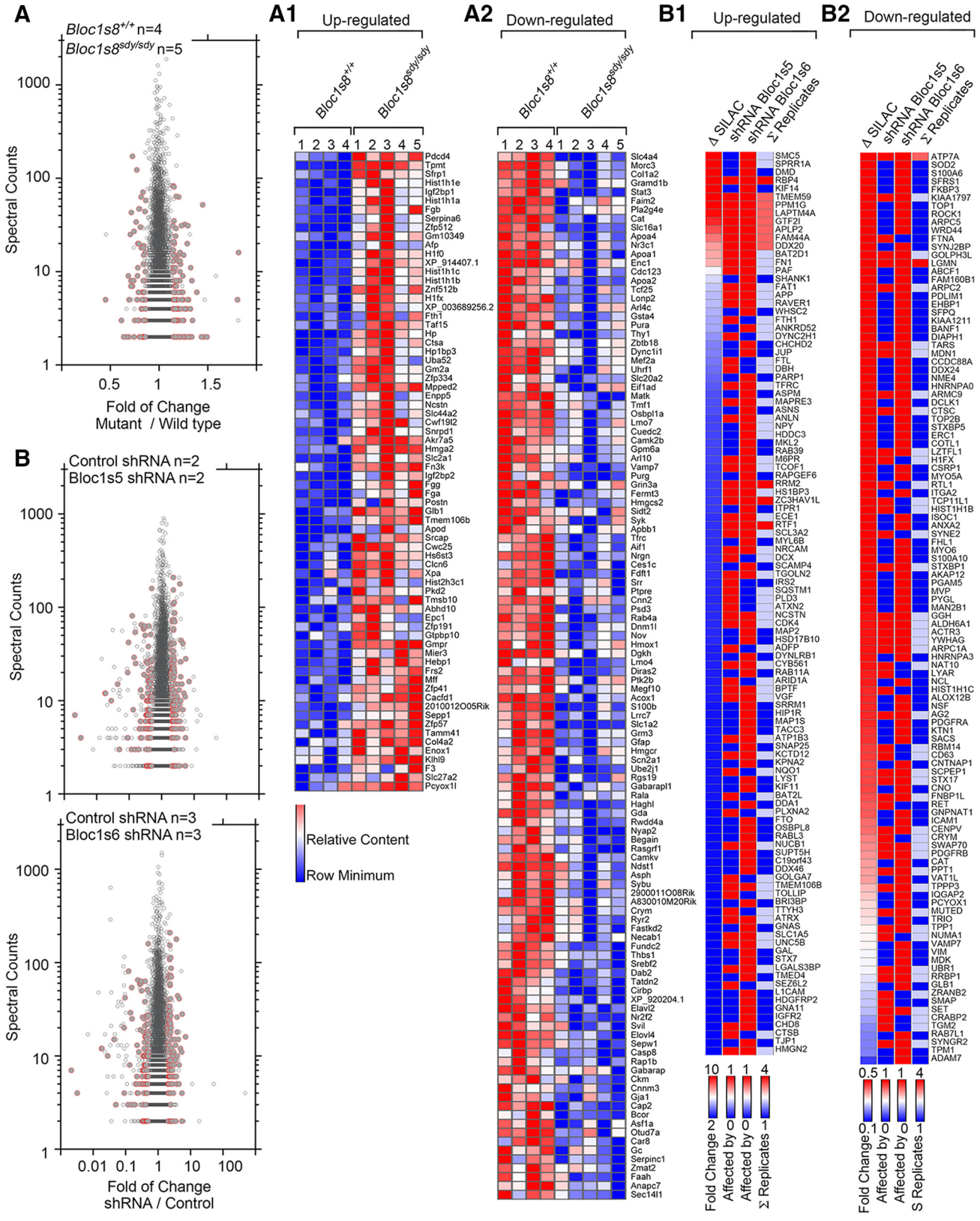

Figure 2. Components of the BLOC-1-sensitive proteome. ***A*–*A2***, Significant TMT proteome hits from wild-type (*Bloc1s8* $^{+/+}$) and dysbindin-null newborn brains (*Bloc1s8* $^{sdy/sdy}$). ***A***, Volcano plot of all TMT protein quantitations. Hits significantly modified by the *Bloc1s8* $^{sdy/sdy}$ are depicted by red-lined circles. ***A1*** and ***A2*** present a hierarchical clustering of the mouse genotypes and changes in protein expression for all significant hits and show upregulated and downregulated proteins, respectively. Each column corresponds to an individual animal. Columns and rows were analyzed using Kendall's tau distance algorithm according to GENE-E (Broad Institute, MIT). ***B*** to ***B2*** present significant SILAC proteome hits from neuroblastoma cells expressing control shRNA and shRNAs directed either to Bloc1s5 muted or Bloc-1s6 pallidin. ***B***, Volcano plots of all SILAC protein quantitations in Bloc1s5 muted or Bloc-1s6 pallidin downregulated cells. Hits significantly modified by BLOC-1 complex subunits downregulation are depicted by red-lined circles. ***B1*** and ***B2*** depict heat maps of proteins upregulated and downregulated by shRNA. Columns present from left to right: fold change, whether a protein was quantified in Bloc1s5– 6 shRNA-treated cells, and the number of independent SILAC experiments in which the protein was quantitated.

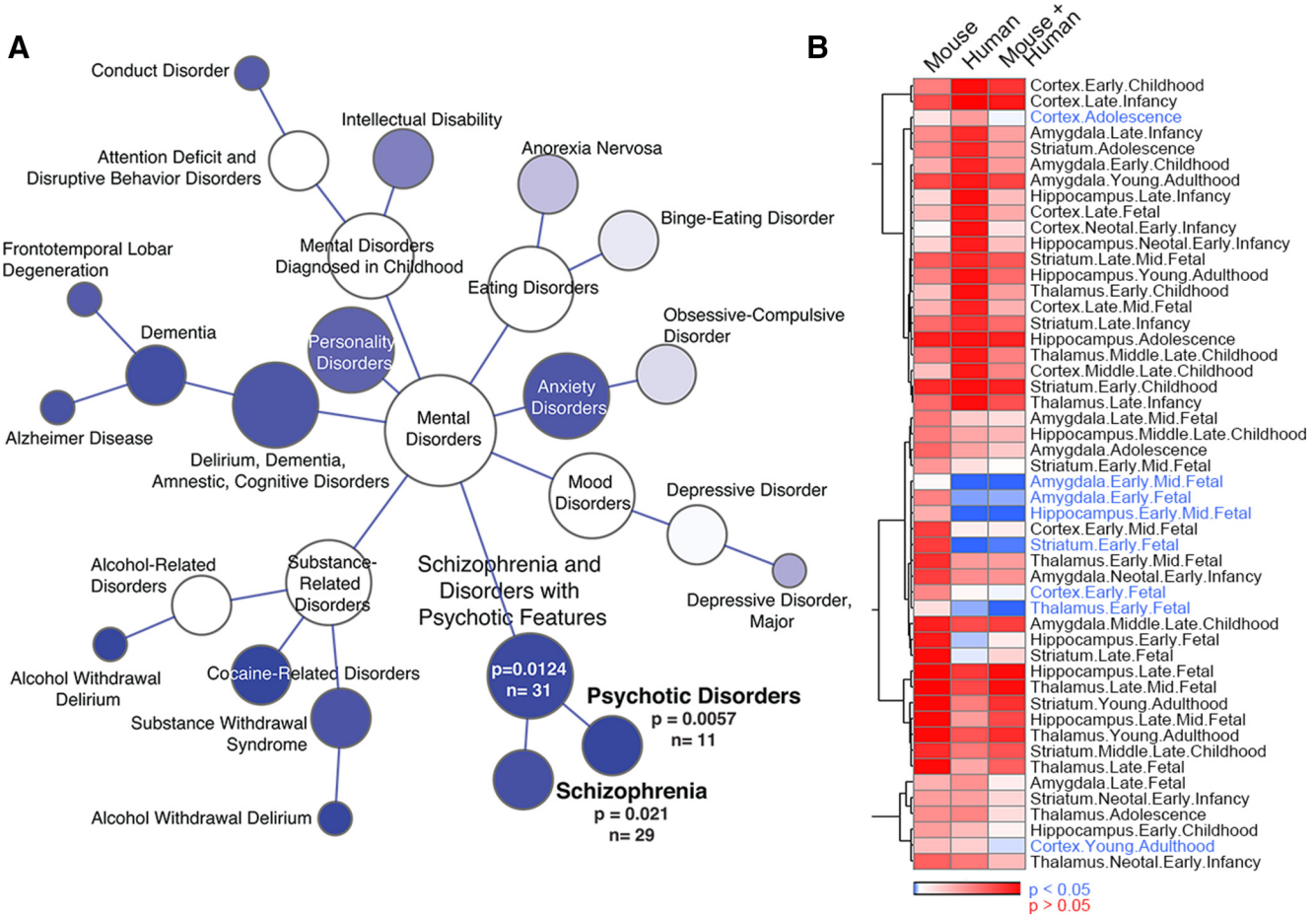

Figure 3. The BLOC-1-sensitive proteome enriches gene products associated with psychiatric disorders and expressed in developing human brain. ***A***, Shown is the analysis of the BLOC-1-sensitive proteome using the GDA algorithm to identify molecular connections between gene sets and diseases (Park et al., 2014; http://gda.cs.tufts.edu/). *p*-values were calculated using 10,000 permutations. Significant hits are depicted with shades of blue. *N* depicts the number of gene products from the BLOC-1-sensitive proteome in the MeSH category. ***B***, BLOC-1-sensitive proteome (mouse + human), *Bloc1s8*$^{sdy/sdy}$-sensitive proteome (mouse), and Bloc1s5–6 shRNA-sensitive proteomes were subjected to expression analysis across brain regions and development using the CSEA algorithm (http://genetics.wustl.edu/jdlab/csea-tool-2/; Dougherty et al., 2010). Columns and rows represent Fisher's exact *p*-values corrected by Benjamini–Hochberg. Data were analyzed by hierarchical clustering using Pearson's correlation according to GENE-E. Significant values are depicted in blue.

convergence and associations (Fontanillo et al., 2011). The human neuroblastoma proteome identified 15 cellular component ontology term metagroups, whereas the mouse proteome identified 13 metagroups (Fig. 4*A*, gray and teal symbols, respectively). Nine of the ontological metagroups were shared between the mouse brain and neuroblastoma proteomes (Fig. 4*A*, red font), indicating that these proteomes do not differ in their GO architecture ($p = 0.151$, two-tailed Fisher's exact probability test).

The five most significant terms within the human sensitive proteome were in order of significance: cytoplasmic membrane-bounded vesicle (GO: 0016023), melanosome (GO: 0042470), neuron projection (GO: 0043005), lysosome (GO: 0005764), and actin cytoskeleton (GO: 0015629). The reliability of this algorithm was determined by the identification of ontology terms defining organelles and cellular compartments in which function or markers are perturbed by BLOC-1 deficiencies. These subcellular compartments include melanosomes, platelet granules, synapse, late endosomes, and lysosomes. The addition of the *Bloc1s8*$^{sdy/sdy}$ brain proteome to the neuroblastoma proteome increased the number of ontological term metagroups to 23 (Fig. 4*A*, blue symbols). Importantly, the top cellular component ontology terms of the BLOC-1-sensitive proteome were shared with those of the mouse brain and neuroblastoma proteome considered in isolation except in their statistical prioritization. In fact, the BLOC-1-sensitive proteome identified the actin cytoskeleton (GO: 0015629; GO: 0043202) as the top ontology term ($p < 10^{-12}$, hypergeometric test; Fig. 4*A*, blue symbols).

We probed the robustness of the BLOC-1-sensitive proteome ontology using two different bioinformatic tools, DAVID and ENRICHR (Fig. 4*B–D*). These tools differ from GeneTerm Linker in their data-processing algorithms (Huang Da et al., 2009; Chen et al., 2013). DAVID identified most GO terms found with GeneTerm Linker either using cellular component or biological process ontology categories (Fig. 4*B*, *C*). Among overlapping terms, cytoskeleton (GO: 0005856) and actin cytoskeleton (GO: 0015629) were significantly represented ($p < 10^{-6}$ and $p < 0.0018$, respectively. Fisher's exact test). Similarly, ENRICHR scored actin binding (GO: 0003779) and SNARE binding (GO: 0000149) as top molecular functions predicted from the BLOC-1-sensitive proteome (combined scores > 12, log *p*-value Fisher's exact test $\times$ *z*-score; Fig. 4*D*). We and others have tested the functional association of the SNARE fusion machinery and the BLOC-1 complex (Ghiani et al., 2010; Dickman et al., 2012; Gokhale et al., 2015b). Therefore, these statistically prioritized ontological categories identify known pathways and/or subcellular compartments in which the BLOC-1 complex resides or is

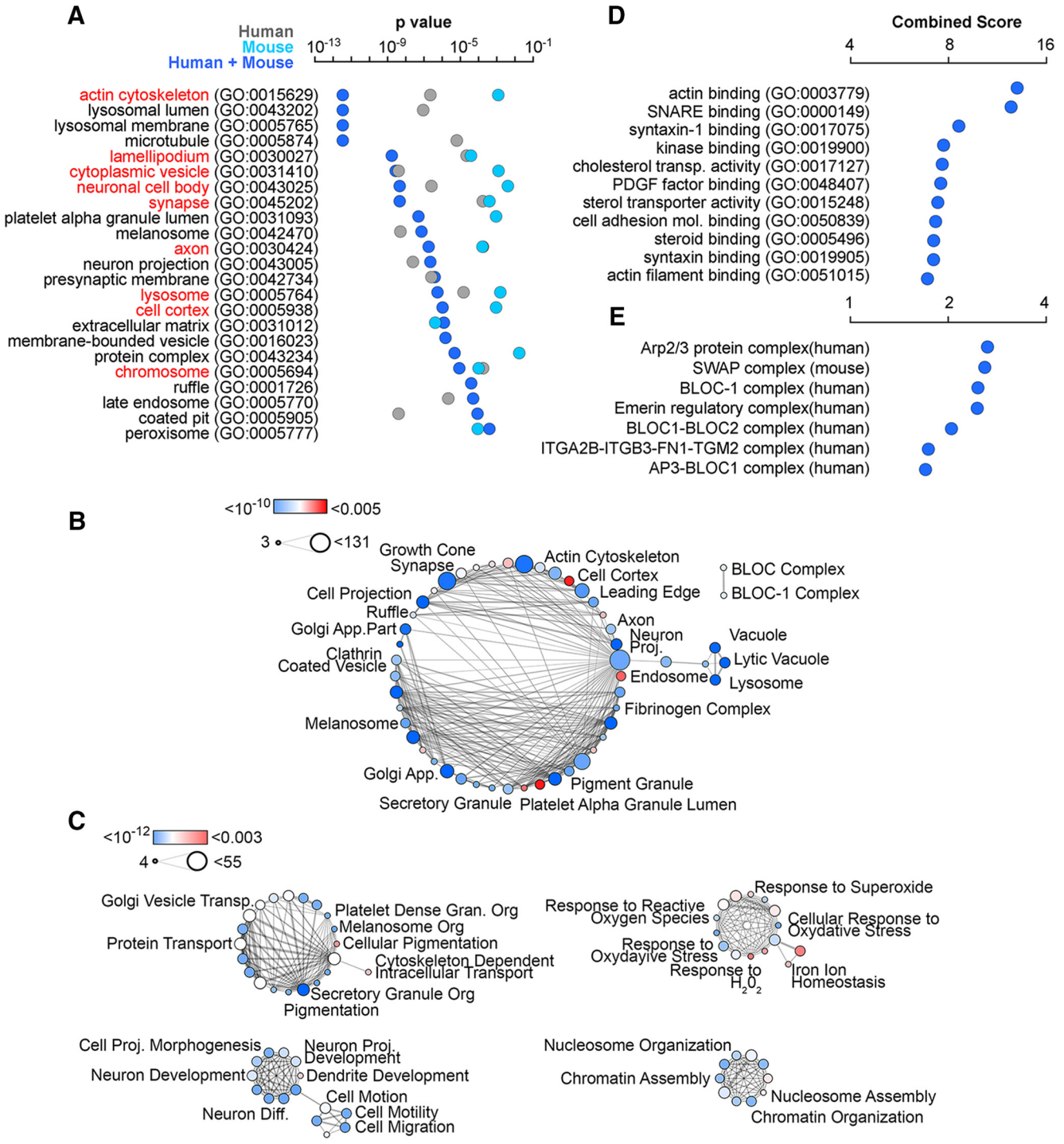

Figure 4. GO analyses of the BLOC-1-sensitive proteome. ***A***, BLOC-1-sensitive proteome (mouse + human, blue symbols), Bloc1s5–6 shRNA-sensitive proteomes (human, gray symbols), and the *Bloc1s8*$^{sdy/sdy}$-sensitive proteome (mouse, teal symbols) were analyzed using the GeneTerm Linker tool (Fontanillo et al., 2011). Nine ontology terms common to mouse and human proteomes are in red font. ***B*** and ***C*** depict the cellular component and biological process GO terms for the BLOC-1-sensitive proteome using the DAVID tool, respectively (Huang Da et al., 2009). Circled area depicts number of gene products from the BLOC-1-sensitive proteome present in the term. Circle color depicts corrected *p*-values, lines and their thickness depict GO terms with the number of shared gene products. ***D*** and ***E*** illustrate GO analysis and the CORUM protein complex analysis of the BLOC-1-sensitive proteome according to ENRICH [combined score = (log *p*-value Fisher's exact test) × (*z*-score); Chen et al., 2013].

required. Ontology strongly argues that the actin cytoskeleton and the BLOC-1 complex belong to a common molecular pathway.

To test whether the actin cytoskeleton and the BLOC-1 complex converge on a shared pathway, we selected molecular targets among the 29 proteins belonging to the actin-binding ontology term (GO: 0003779; Fig. 4*D*). We determined previously that the WASH complex and annexin A2 (ANXA2) interact with the BLOC-1 complex to regulate the actin cytoskeleton at endosomes (Ryder et al., 2013; Delevoye et al., 2016). We found downregulated ANXA2 within the BLOC-1-sensitive proteome (Fig. 2*B2*). Annexin A2 and the WASH complex activate the Arp2/3 actin

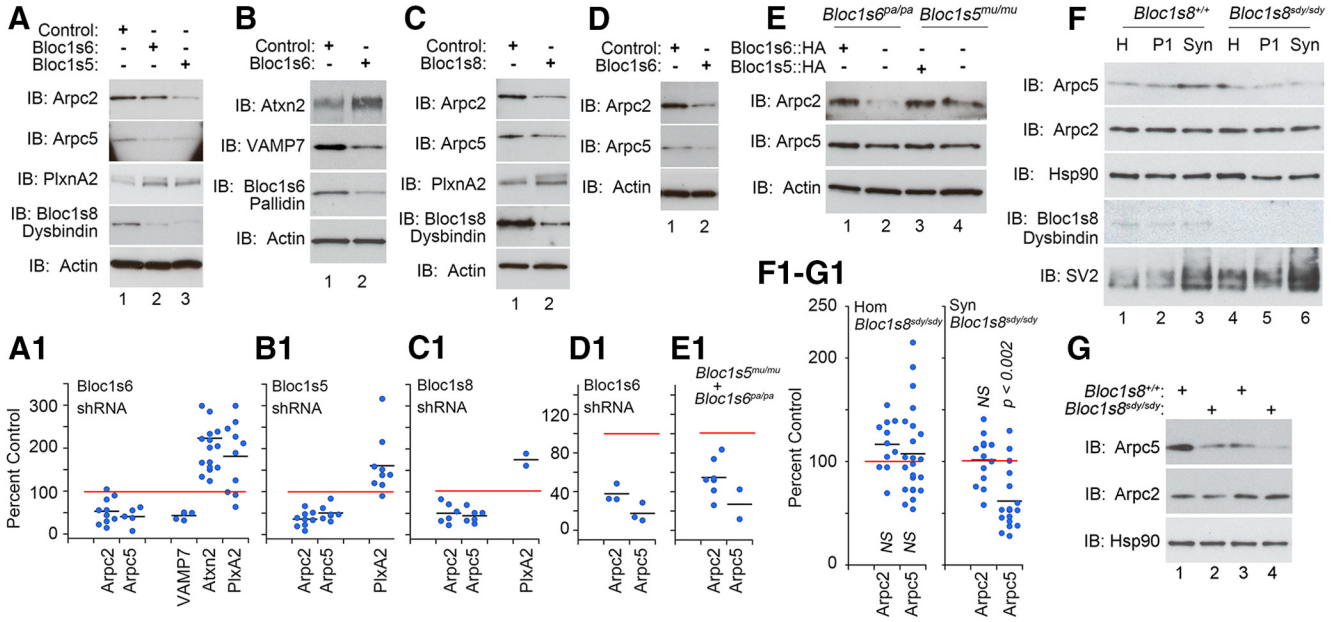

Figure 5. The Arp2/3 actin polymerization complex is downregulated after BLOC-1 loss-of-function. ***A–C***, SH-SY5Y cells were treated with control or shRNAs against either one of three BLOC-1 subunits (Bloc1s5, 6, and 8) and cell extracts analyzed by immunoblot with antibodies against the BLOC-1-sensitive proteome components: Arp2/3 complex subunits (Arpc2 and 5), ataxin 2 (Atxn2), and plexin A2 (PlxnA2). Antibodies against actin, BLOC-1 subunits, and the BLOC-1-sensitive SNARE VAMP7 were used as controls. ***D***, MNT1 melanoma cells were treated with control or Bloc1s6 shRNAs and cell extracts analyzed as in ***A***. ***E***, Immortalized melanocytes from mouse mutants carrying null mutations in the BLOC-1 subunits Bloc1s5–6 (*Bloc1s5*$^{mu/mu}$ and *Bloc1s6*$^{pa/pa}$) or cells rescued by expression of the missing subunit were analyzed as in ***A***. ***F***, ***G***, Synaptosomes of six wild-type and six *Bloc1s8*$^{sdy/sdy}$ hippocampi were analyzed. ***F***, ***G***, Three independent fractionations. In ***F***, all fractions are depicted (H, homogenate and P1, low speed pellet), whereas in ***G***, only synaptosomes are shown. Samples were probed by immunoblot with Arpc2 and 5 antibodies, hsp90 as loading control, dysbindin, and the synaptic vesicle marker SV to indicate synapse enrichment. ***A1–G1***, Dot plots representing the protein expression normalized to the control genotype. Each dot depicts an independent determination from at least three independent experiments. Red line marks 100%. All quantitations in ***A1*** to ***E1*** were significantly different from actin. In ***F1*** and ***G1***, only Arpc5 was significantly different compared with controls with hsp90 (***F***, ***G***). Significance was determined by Kruskal–Wallis test followed by Wilcoxon Mann–Whitney nonparametric tests.

polymerization complex, suggesting that the Arp2/3 complex could be a downstream BLOC-1 pathway component. We used the ENRICHR tool to prioritize statistically complexes curated in the CORUM database of protein complexes (Fig. 4*E*; Ruepp et al., 2010). The top ranked predicted complex was Arp2/3 represented by four of its seven subunits (ACTR3, ARPC1A, ARPC2, ARPC5; combined score = 2.64). These four Arp2/3 subunits were putatively downregulated in the BLOC-1-sensitive proteome (Fig. 2*B2*). The SWAP and the BLOC-1 complexes closely scored with the Arp2/3 complex (combined scores = ~2.5). The SWAP complex was implicated in B-cell-specific Ig gene recombination, yet one of its subunits, SWAP-70, binds directly to actin and acts as a guanine-nucleotide-exchange factor required for actin-dependent membrane ruffling (Borggrefe et al., 1998; Shinohara et al., 2002; Ihara et al., 2006).

Arp2/3 complex expression is reduced in BLOC-1 deficiency

We confirmed the effects of BLOC-1 loss of function on the expression of Arp2/3 complex subunits in diverse cells and hippocampal fractions enriched in synapses, also called synaptosomes (Fig. 5). We used antibodies against the Arp2/3 subunits Arpc2 and Arpc5 to measure Arp2/3 complex levels and contrasted these results with VAMP7, a protein with expression that is reduced in BLOC-1 deficiencies (Salazar et al., 2006; Newell-Litwa et al., 2010). Arpc2 and Arpc5 expression was consistently downregulated in all cells regardless of whether BLOC-1 was downregulated with shRNAs against Bloc1s5, 6 or 8 in neuroblastoma cells (Fig. 5*A–C1*). Similarly, the shRNA against Bloc1s6 reduced Arpc2 and 5 expression regardless of whether the shRNA-treated cells were SH-SY5Y neuroblastoma (Fig. 5*A–C1*) or MNT-1 melanoma cells (Fig. 5*D–D1*). We measured the levels of Arpc2 and 5 in immortalized melanocytes isolated from mice carrying null mutations of *Bloc1s5* and *6*, *Bloc1s5*$^{mu/mu}$, and *Bloc1s6*$^{pa/pa}$ (Fig. 5*E–E1*). Arpc2 and 5 expression was increased by rescuing these mutants cells with cDNAs encoding the missing subunits (Fig. 5*E*, cf. even and odd lanes). These results demonstrate that reduced levels of BLOC-1 complex decrease the expression levels of Arp2/3 subunits in diverse cell lines.

We assessed whether Arp2/3 complex subunits expression was affected in adult dysbindin-null *Bloc1s8*$^{sdy/sdy}$ mouse hippocampus and synaptic enriched fractions. Arpc2 and Arcp5 expression was not altered in total brain or hippocampal homogenates from adult *Bloc1s8*$^{sdy/sdy}$ mice (Fig. 5*F*, lanes 1 and 4, *F1*). However, Arpc5 expression was reduced by 50% in synaptosomes from *Bloc1s8*$^{sdy/sdy}$ hippocampus. The synaptic vesicle marker SV2 was used to determine the extent of synaptic enrichment in synaptosome fractions (Fig. 5*F*, *G*). In contrast with Arpc5, Arpc2 levels were not affected by the *Bloc1s8*$^{sdy/sdy}$ allele compared with wild-type synaptosomes and a loading control, Hsp90 (Fig. 5*F*, lanes 3 and 6, *G*, cf. even and odd lanes and *G1*). These results indicate that expression of selected subunits of the Arp2/3 complex is decreased in synaptic enriched fractions of adult dysbindin-null hippocampus. Collectively, these results show that the integrity of the BLOC-1 complex is required to maintain the expression of subunits of the Arp2/3 complex. Furthermore, our results confirm that GO distillation of the BLOC-1-sensitive proteome reliably and robustly identifies a molecular pathway converging on BLOC-1.

The WASH complex is an Arp2/3 activator that resides in endosomes and interacts with the BLOC-1 complex (Seaman et al., 2013; Ryder et al., 2013). We measured the levels of BLOC-1, Arp2/3 complex subunits, and ataxin 2 to determine whether the BLOC-1 complex was the most upstream component on a path-

way interacting with the Arp2/3 complex via the WASH complex. We used control mouse fibroblasts in which the *Wash1* gene was engineered as a flox conditional allele ($WASH^{f/f}$) and null cells in which *Wash1* was excised with cre recombinase ($WASH^{-/-}$; Gomez et al., 2012). We confirmed the excision of the *Wash1* gene measuring the expression of two subunits of the WASH complex, strumpellin and FAM21, the expression of which was reduced by ~50% (Fig. 6; Gomez et al., 2012). Moreover, and similar to what we observed in BLOC-1-deficient cells and synaptosomes, the expression of the Arp2/3 subunit Arpc5 and ataxin were significantly downregulated and upregulated, respectively (Fig. 6). These changes in two BLOC-1-sensitive proteins occurred even though the BLOC-1 complex was unaffected in WASH-null cells, as measured by the expression of the BLOC-1 subunits Bloc1s6 (pallidin) and Bloc1s8 (dysbindin) (Fig. 6). These results support a model in which the BLOC-1, WASH, and Arp2/3 complexes are organized sequentially on a pathway. We further tested a pathway model to investigate whether BLOC-1, WASH, and Arp2/3 complexes could coprecipitate. We found previously that BLOC-1 and WASH complexes coimmunoprecipitate with antibodies against recombinant FLAG-tagged dysbindin expressed in SH-SY5Y neuroblastoma cells (Ryder et al., 2013). FLAG-tagged dysbindin precipitated the BLOC-1 complex subunit Bloc1s6 pallidin, along with the WASH subunits strumpellin and FAM21 and the Arp2/3 subunit Arpc2 (Fig. 6*D*, lane 1). Importantly, reverse immunoprecipitations with antibodies against Arpc2 brought down the BLOC-1 complex subunit Bloc1s6 pallidin (Fig. 6*E*, lane 1). In these experiments, we excluded spurious binding of BLOC-1, WASH, and Arp2/3 subunits to bead–antibody complexes with either addition of an excess FLAG peptide to immunoprecipitates (Fig. 6*D*, lane 2) or using beads decorated with an anti-HA antibody (Fig. 6*E*, lane 2). Further probing of Arpc2 immunoprecipitates with antibodies against strumpellin and FAM21 was precluded because all antibodies are raised in the same species. We conclude that BLOC-1 and Arp2/3 form complexes that include Arp2/3 activators such as the WASH complex establishing a sequentially organized pathway.

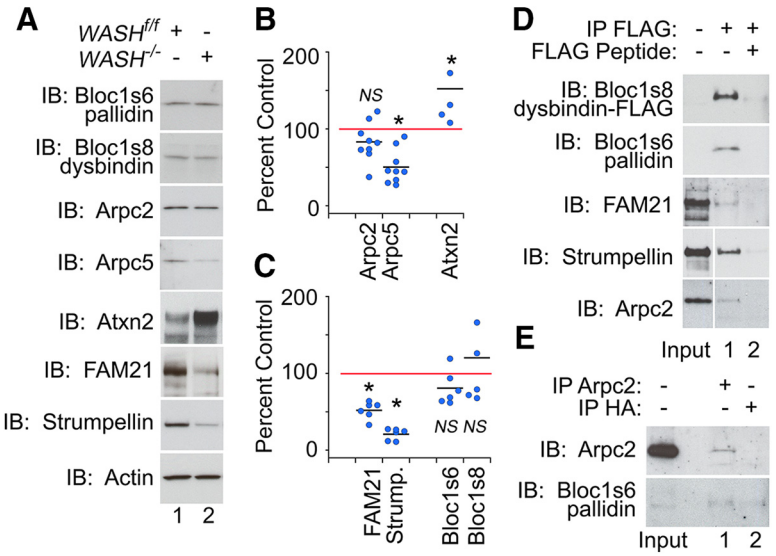

Figure 6. Genetic and biochemical interactions of the BLOC-1, WASH, and Arp2/3 complexes. ***A***, Control ($WASH^{f/f}$) and WASH-null ($WASH^{-/-}$) mouse embryonic fibroblast cell extracts were analyzed by immunoblot with antibodies against the BLOC-1-sensitive proteome components Arp2/3 complex subunits (Arpc2 and 5) and ataxin 2 (Atxn2), as well as antibodies against actin, BLOC-1 subunits (Bloc1s6 and 8), and the WASH complex subunits strumpellin and FAM21. ***B***, Dot plots representing the protein expression normalized to the control genotype. Each dot represents an independent determination from three or four independent experiments. Red line marks 100%. *p*-values were obtained by comparing against actin using the Kruskal–Wallis test followed by Wilcoxon Mann–Whitney nonparametric tests. Arpc2 and BLOC-1 subunits were not significant (NS). Asterisks mark all significant values ($p < 0.0017$). ***D***, ***E***, Immunoprecipitations of FLAG-tagged dysbindin expressed in SH-SY5Y cells (***D***) or immunoprecipitations with Arpc2 antibodies (***E***). BLOC-1 complex was detected by immunoblot of the precipitated complexes with antibodies against FLAG or pallidin, WASH complexes were revealed by blotting with antibodies against strumpellin and FAM21; the Arp2/3 complex was detected with antibodies against Arpc2 (***D***, ***E***, $n = 3$).

Arp2/3 and BLOC-1 complexes interact

Our hypothesis that the Arp2/3 complex and BLOC-1 participate in a common pathway makes three testable predictions that we focused on. First, the dynamic of actin filaments should be impaired in compartments in which the BLOC-1 complex normally resides. Second, genetic deficiencies in BLOC-1 should phenocopy mutations in subunits of the Arp2/3 complex. Finally, transheterozygotic mutations either between two distinct BLOC-1 subunits or one BLOC-1 and Arp2/3 subunits should generate similar phenotypic outcomes.

We measured actin dynamics using fluorescent recovery after photobleaching (FRAP) of the F-actin probes Lifeact-RFP and actin-GFP expressed in the same cells (Fig. 7; Riedl et al., 2008). We expressed these probes in cells carrying an exofacially FLAG tagged β-adrenergic receptor in which endocytosis is induced by the agonist isoproterenol. Isoproterenol-induced receptor internalization allowed us to define precisely early endosomes functionally (Fig. 7*C*). The dynamics of endosome localized actin filaments was similarly reported by Lifeact-RFP and actin-GFP (Fig. 7*A*). Moreover, both probes experienced negligible bleaching due to imaging (Fig. 7*B*). Therefore, we focused on Lifeact-GFP because actin-GFP is partially functional (Doyle and Botstein, 1996; Deibler et al., 2011). We demonstrated previously that the size and tubulation of β-adrenergic receptor-positive endosomes is increased by BLOC-1 downregulation (Puthenveedu et al., 2010; Ryder et al., 2013). We transduced cells with control and Bloc1s6 shRNA lentiviruses to downregulate BLOC-1 complexes. LifeAct labeled discrete actin-positive domains in the limiting membrane of early endosomes, which were identified by the presence of FLAG antibodies internalized after 10 min of isoproterenol addition (Fig. 7*C*). These actin spots rapidly recovered their LifeAct FRAP in control cells (Fig. 7*D*,*E*). In contrast, FRAP was significantly reduced in BLOC-1-downregulated cells compared with control shRNA-treated cells (Fig. 7*D*,*E*). These results demonstrate that actin dynamics at early endosomes is decreased in cells in which the function of the BLOC-1 is impaired.

Drosophila Arp2/3 and BLOC-1 complexes interact genetically

We tested our hypothesis that the Arp2/3 complex and BLOC-1 participate in a common pathway with a genetic analysis of the *Drosophila* third-instar larva neuromuscular junction (NMJ) (Fig. 8) and *Drosophila* DA neurons focusing on the morphologically distinct Class-IV (C-IV) DA neurons. We chose the NMJ

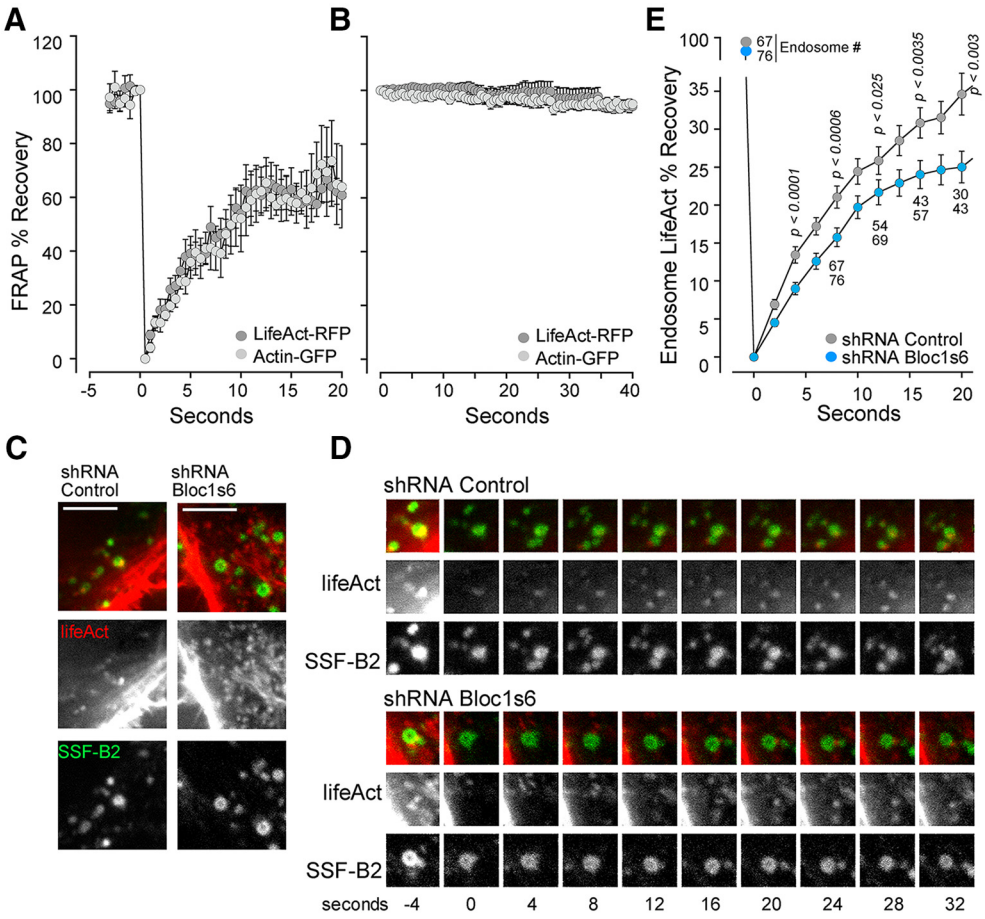

Figure 7. Filamentous actin dynamics are reduced in endosomes of BLOC-1-downregulated cells. HEK293 cells expressing the β-adrenergic receptor tagged with exofacial FLAG tag were transfected with LifeAct-RFP and Actin-GFP and the receptor was induced to internalize with isoproterenol for 10 min. Receptor internalization was followed with fluorescently labeled FLAG antibodies. ***A***, FRAP of LifeAct-RFP and Actin-GFP localized to early endosomes identified by internalized receptors tagged with FLAG antibodies (endosomes not shown). ***B***, Presents bleaching of both probes due to imaging. ***C–E***, Control scramble (gray symbols, ***E***) and Bloc1s6 shRNA-treated HEK293 cells expressing LifeAct-GFP and a N-terminal FLAG tagged β-adrenergic receptor (teal symbols, ***E***) were imaged after inducing early endosome labeling with fluorescent FLAG antibodies (SSF-B2) and isoproterenol for 10 min. ***D***, ***E***, Endosome LifeAct-GFP signal was bleached and FRAP measured as described. ***E***, *p*-values were obtained by comparing scrambled and Bloc1s6 shRNA-treated cells at specific time points after photobleaching using the Kruskal–Wallis test followed by Wilcoxon Mann–Whitney nonparametric tests. Numbers under symbols depict the number of endosomes quantified per condition and collected in three independent experiments.

synapse because it doubles its synaptic bouton numbers in BLOC-1 loss-of-function mutations (Mullin et al., 2015). We selected the C-IV DA neurons because their dendritic arbor is sensitive to genetic disruption of actin cytoskeleton components and their terminal branches are enriched in actin (Andersen et al., 2005; Jinushi-Nakao et al., 2007; Iyer et al., 2012; Ferreira et al., 2014). We focused on mutants in the orthologs of mammalian Bloc1s1, 6, and 8, which are encoded by the *Drosophila* genes *blos1*, *pldn*, and *dysb*. The products of these *Drosophila* genes assemble into a bonafide BLOC-1 complex (Cheli et al., 2010; Mullin et al., 2015). We first resolved a discrepancy of reported bouton count phenotypes in BLOC-1 mutants (Dickman and Davis, 2009; Mullin et al., 2015) and tested whether food composition is a source of these differences. We raised our stocks on our food and the food used by Dickman and Davis (2009), herein referred to as DD food (Fig. 8*A*,*C*). The DD food caused an increase in the number of boutons in wild-type w^{1118} flies that was identical to the number of boutons observed in all BLOC-1 mutant animals regardless of the food on which they were grown (Fig. 8*B*,*D*,*E*). The low bouton count observed in our wild-type w^{1118} animals raised on our food was also observed in two additional w^{1118} independent stocks of wild-type flies, c^{155} animals and the w^{1118} animals used in Dickman and Davis (2009), thus excluding genotypic differences in our stocks (Fig. 8*B* and data not shown). Importantly, the $dysb^{1}$ increased bouton count phenotype could be rescued by the expression of a UAS-Dysb-Venus transgene driven by the c^{155} neuronal GAL4 driver (Fig. 8*B*,*D*).

We used this robust bouton count morphological assay to test whether *Drosophila* BLOC-1 and Arp2/3 mutant alleles phenocopy each other. Homozygous mutant $blos1^{ex65}$, $pldn^{-}$, and $dysb^{1}$ animals significantly increased their synaptic bouton counts compared with control w^{1118} animals (Fig. 8*B*,*D*,*E*). The increased bouton phenotype observed in $blos1^{ex65}$ and $dysb^{1}$ mutants alleles is equally severe in heterozygous and homozygous animals (Fig. 8*B*,*D*,*E*; Mullin et al., 2013). As predicted, the increased synaptic bouton phenotype was also evident in two lethal alleles of the *Drosophila* Arp2/3 subunit Arpc1 when introduced as heterozygous mutations, $Arpc1^{Q25st/+}$ and $Arpc1^{Q25sd/+}$ (Fig. 8*B*,*E*; Hudson and Cooley, 2002). These results demonstrate that mutations in BLOC-1 complex and Arp2/3 subunits phenocopy each other at the neuromuscular synapse, suggesting they converge on a common mechanism.

The synaptic bouton phenotype of *blos1* heterozygous animals is suppressed when combined with other loss-of-function alleles of another BLOC-1 subunit (Mullin et al., 2013). This observation offers a powerful assay to test whether BLOC-1 and Arp2/3

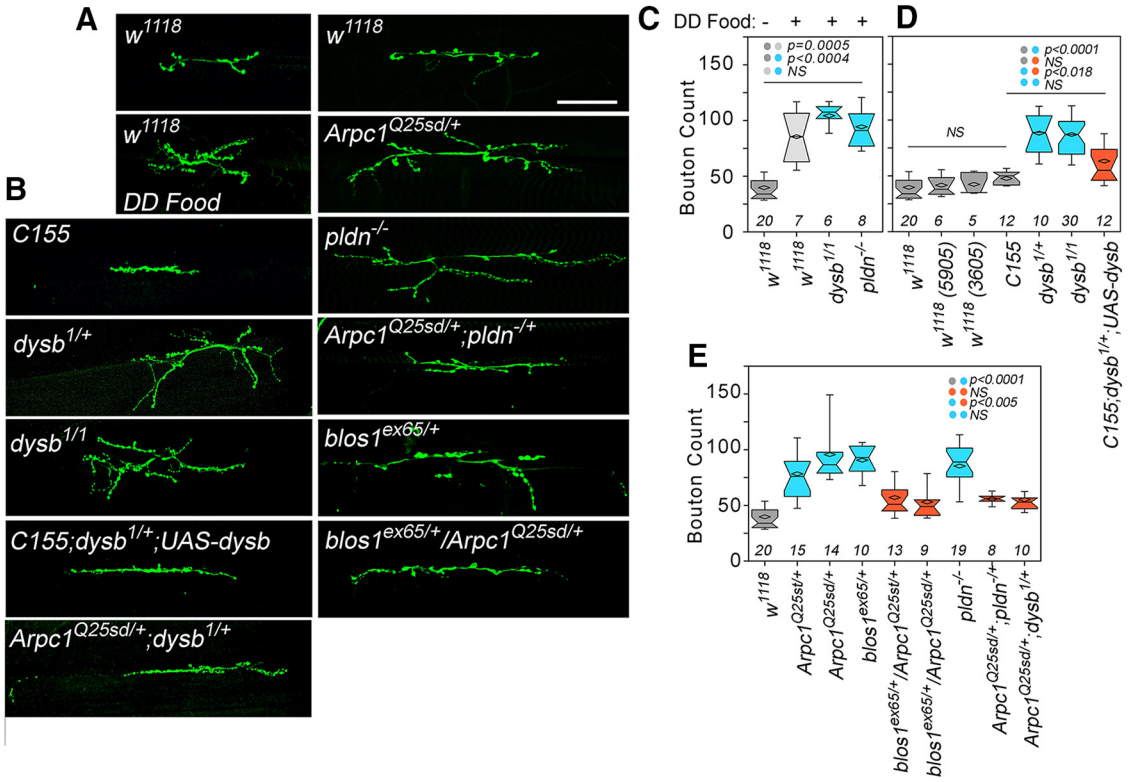

Figure 8. The *Drosophila* BLOC-1 and Arp2/3 complexes genetically interact in the synapse. ***A***, ***B***, *Drosophila* third-instar larva NMJs were stained with HRP antibodies to label nerve terminals in wild-type (***A***, ***B***; w^{1118}; ***D***, three different stocks of w^{1118} or c^{155}), BLOC-1-deficient animals (***B–E***; $pldn^{-/-}$, $dysb^{1}$, $blos1^{ex65}$), two null alleles in the Arp2/3 complex (***B–E***, $Arpc1^{Q25st/+}$ and $Arpc1^{Q25sd/+}$), and transheterozygotes of the BLOC-1 subunits alleles and one of two *Arpc1* alleles. ***A***, Images of synapses of animals raised in our food (− symbol in ***C***) and DD food (Dickman and Davis, 2009) with bouton counts in ***C***. ***C–E***, Bouton counts are presented as box plots where the box indicates percentiles 25th and 75th. Box line represents sample median and diamonds sample mean, notches mark the half-width. Numbers of animals per genotype are in the abscissa in italics. Comparisons were made by the Kruskal–Wallis test followed by Wilcoxon Mann–Whitney nonparametric tests.

complexes converge on a pathway. Transheterozygotic animals carrying one copy of $blos1^{ex65}$ and either one of the *Arpc1* alleles indeed suppressed the phenotype observed in each one of these deficiencies in isolation (Fig. 8*B*,*E*). The same suppression of the bouton phenotype was observed in transheterozygotic animals carrying one copy of $pldn^{-}$ or $dysb^{1}$ in combination with $Arpc1^{Q25sd/+}$ (Fig. 8*B*,*E*). All transheterozygotic synaptic bouton counts were similar to wild-type w^{1118} flies and were also significantly different from each one of the mutant alleles in isolation (Fig. 8*B*,*E*). We observed no differences in the size of the target muscle by a 50% reduction in Arpc1 dosage (data not shown), an observation consistent with the reported lack of effect of Arp2/3 either in assembly of actin filaments or contraction in differentiated striated muscle (Pollard et al., 2002). These results indicate that the BLOC-1 and Arp2/3 complexes converge on a pathway to regulate synapse morphology.

We tested whether genetic interactions between BLOC-1 and Arp2/3 complexes were similar in dendrites and NMJ terminals. Therefore, we studied the *Drosophila* third-instar larvae C-IV DA neurons. These neurons possess an elaborate and stereotypic dendritic arbor with a complexity that is sensitive to genetic perturbation of actin modulators (Andersen et al., 2005; Jinushi-Nakao et al., 2007; Iyer et al., 2012; Ferreira et al., 2014). We investigated whether hemideficiencies in *Arpc1* and the BLOC-1 subunits *blos1* and *dysb* could alter the dendritic arborization of these neurons. Mutant *blos1* and *dysb* decreased the number of dendrite branches and the total dendrite length per neuron (Fig. 9*A*,*C*,*D*). These *blos1* and *dysb* mutant phenotypes were more pronounced in the actin-rich terminal branches, as demonstrated by the reversed Strahler analysis, in which branches of the 1 and 2 categories (i.e., terminals) were the most affected (Fig. 9*E*). Branches closer to the cell body were not significantly affected in these BLOC-1 hemideficiencies (Fig. 9*E*; Strahler categories 3–8). In contrast, the dendritic arbor was not affected in $Arpc1^{Q25sd/+}$ C-IV DA neurons (Fig. 9*A*,*C–E*). With respect to genetic interactions between BLOC-1 and Arp2/3 complexes in C-IV dendrites, haploinsufficiency dendritic phenotypes observed in $blos1^{ex65}$ were further enhanced by the transheterozygotic $Arpc1^{Q25sd}$ allele in the case of the total number of branches (Fig. 9*A*,*C*); however, the haploinsufficiency phenotypes observed in $dysb^{1}$ were not modified by the transheterozygotic $Arpc1^{Q25sd}$ allele (Fig. 9*A*,*C–E*). We confirmed that the C-IV DA neurons' dendritic arbor indeed cell autonomously requires the Arp2/3 complex by creating $Arpc1^{Q25sd}$ homozygous-null mutant clones in sensory neurons using MARCM (Fig. 9*B*,*F*). $Arpc1^{Q25sd}$ mutant C-IV MARCM clones exhibited drastically decreased complexity of the dendritic tree, indicating that the Arp2/3 complex is necessary for normal dendritic development of sensory neurons (Fig. 9*B*,*F*). These results demonstrate that BLOC-1 and Arp2/3 complexes are required for dendritic development by mechanisms that differ between presynaptic and dendritic compartments.

Arp2/3 and BLOC-1 modulate presynaptic plasticity

Mutations in *dysb* block a philanthotoxin-induced homeostatic increase in quantal content that maintains muscle response during evoked potentials. This adaptive synaptic response is localized to the presynaptic compartment (Dickman and Davis, 2009; Dickman et

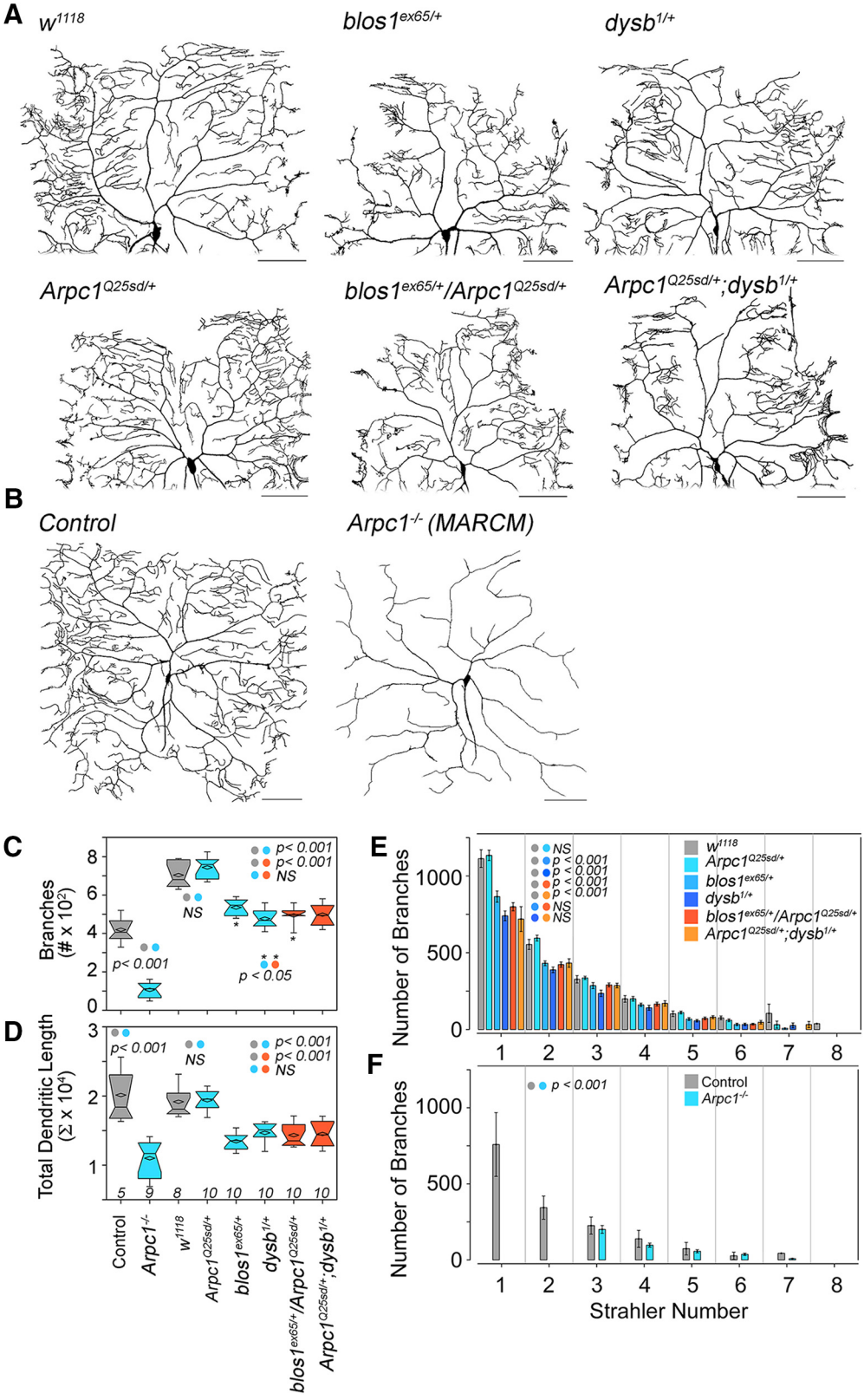

Figure 9. The *Drosophila* BLOC-1 and Arp2/3 complexes affect dendritic morphology in C-IV DA neurons. ***A***, Representative live confocal images of C-IV DA neurons of the specified genotypes labeled by *ppk-EGFP*. ***B***, Control and *Arpc1*-null C-IV neurons generated by MARCM (*Arpc1*$^{-/-}$). Scale bars in ***A*** and ***B*** correspond to 100 μm. ***C*** and ***D*** show quantitative analysis of total number of dendritic branches and total dendritic length in the specified genotypes. Data are presented as box plots where the box indicates percentiles 25th and 75th. Box line represents sample median and diamonds sample mean, notches mark the half-width. ***E*** and ***F*** depict reversed Strahler branch analysis that shows that BLOC-1 haploinsufficiency phenotypes significantly affect terminal actin rich branches (Strahler number 1 and 2). Comparisons were made by the Kruskal–Wallis test followed by Wilcoxon Mann–Whitney nonparametric tests. Numbers of animals per genotype in ***C***–***F*** are in the abscissa in italics in ***D***.

al., 2012; Gokhale et al., 2015b). We used this *dysb* sensitive phenotype to determine whether an interaction between Dysbindin and the Arp2/3 complex could modulate presynaptic mechanisms. As reported previously, exposure to philanthotoxin did not affect evoked potentials (EJP) after 10 min of toxin addition in wild-type w^{1118} animals (Fig. 10*A*). In contrast, the EJP amplitude was decreased in the $dysb^{1}$ flies after toxin addition, a reflection of decreased quantal content compared with w^{1118} (Fig. 10*A*,*C*). As described previously, single alleles of $dysb^{1}$ or $blos1^{ex65}$ did not affect the response to philanthotoxin (Fig. 10*C*; Dickman and Davis, 2009; Dickman et al., 2012; Gokhale et al., 2015b). Single-copy loss of *arpc1* ($Arpc1^{Q25sd/+}$) phenocopied the $dysb^{1}$ impaired response after toxin addition (Fig. 10*A*,*C*). We tested whether this *arpc1*-dependent phenotype was presynaptic by analyzing transheterozygotic animals harboring one copy of $blos1^{ex65}$ or $dysb^{1}$ in combination with $Arpc1^{Q25sd/+}$. Simple copy loss of these two BLOC-1 subunits reverted the decreased $Arpc1^{Q25sd/+}$ plasticity phenotype to levels close to wild-type w^{1118} (Fig. 10*A*,*C*). None of these effects was due to differences in the response of synapses to philanthotoxin. All animals decreased the amplitude of spontaneous fusion events (mEJP) by 50% after toxin addition (Fig. 10*B*). These results demonstrate that subunits of the BLOC-1 complex interact with components of the Arp2/3 complex to modulate an adaptive synaptic response. Collectively, our findings demonstrate that ontologies derived from proteomes sensitive to single gene defects inform the formulation of novel schizophrenia mechanistic hypotheses converging at the synapse.

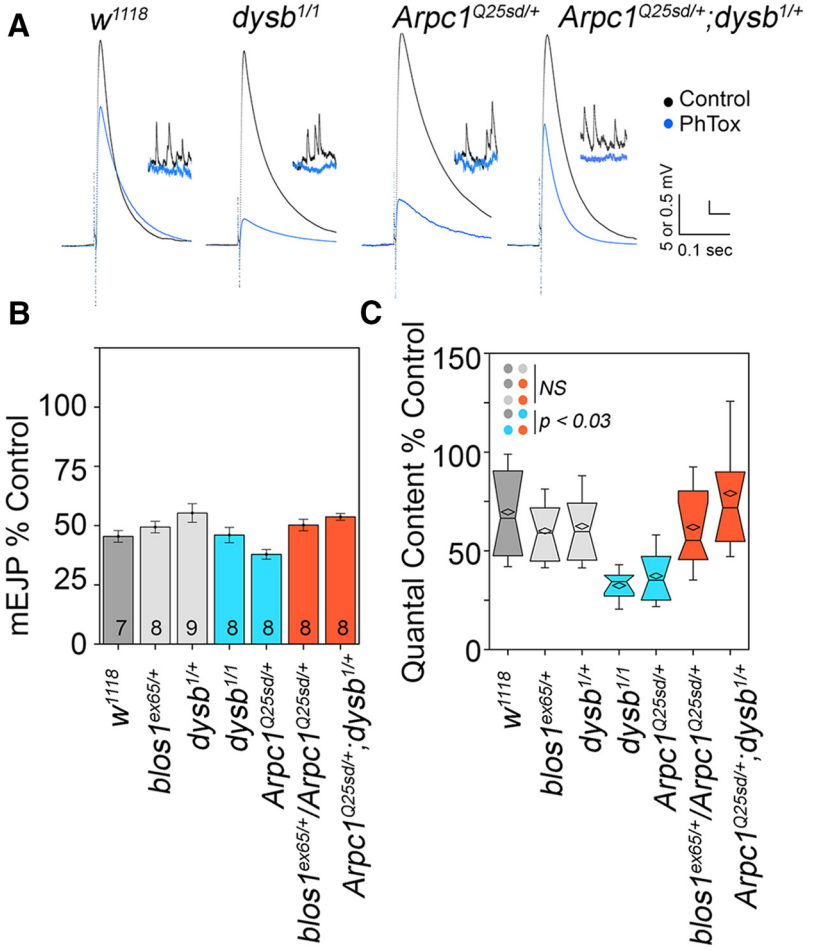

Figure 10. *Drosophila* dysbindin and Arp2/3 complexes interact to modulate homeostatic synaptic plasticity. ***A***, Representative EJP and mEJP traces without philanthotoxin-433 (PhTx, black) and after PhTx incubation (blue). ***B***, mEJP amplitude after philanthotoxin-433 addition (average and SEM). ***C***, Quantal content across different genotypes. Data are presented as box plots where the box indicates percentiles 25th and 75th. Box line represents sample median and diamonds sample mean, notches mark the half-width. Numbers of animals per genotype are in the abscissa. Comparisons were made by the Kruskal–Wallis test followed by Wilcoxon Mann–Whitney nonparametric tests.

Discussion

We used global quantitative proteome profiling and GO to identify and prioritize unbiasedly pathways altered by defect in single genes implicated in neurodevelopmental disorders. We used this strategy in neuronal cells and in tissue with reduced expression of one of three BLOC-1 subunits: Bloc1s5 (muted), Bloc1s6 (pallidin), and Bloc1s8 (dysbindin). Our goal was to identify effectors downstream of the BLOC-1 complex and proteins belonging to compensatory mechanisms activated by BLOC-1 genetic defects. The neuronal BLOC-1-sensitive proteome satisfies three criteria. First, the proteome sensitive to BLOC-1 deficiencies enriches gene products and ontological terms implicated in psychosis and schizophrenia risk (Fig. 3). Second, the proteome is modularly organized into discrete GO categories. These ontology categories include known and novel pathways sensitive to BLOC-1 genetic defects (Fig. 4). Finally, prioritization of the proteome by GO brought into focus the Arp2/3 complex, which we demonstrate interacts genetically with the BLOC-1 complex at a *Drosophila* model synapse, the larval NMJ (Fig. 8).

Whole-brain Bloc1s8-null proteome poorly overlapped with the proteome of neuroblastoma cells downregulated for BLOC-1 subunits likely because of a low discovery rate of isolated proteomes. However, the ontological organization of the human or mouse brain proteomes did not differ statistically. In fact, the addition of the brain proteome to the proteome of the BLOC-1 downregulated human neuroblastoma cells, the BLOC-1-sensitive proteome, improved the significance of common GO terms identified by the mouse brain and human neuroblastoma considered in isolation. We distilled the BLOC-1-sensitive proteome into two statistically prioritized GO terms, actin cytoskeleton (GO: 0015629) and actin binding (GO: 0003779). Among the actin binding proteins in GO: 0003779 (Fig. 4*D*), the protein content of which has been reported to be reduced in dysbindin-BLOC-1-null cells or brain. These include the Arp2/3 activator annexin A2 (ANXA2), synapsin 1 (SYN1), and a subunit of calcium/calmodulin-dependent protein kinase II (CAMK2B; Numakawa et al., 2004; Morel et al., 2009; Fei et al., 2010; Borgesius et al., 2011; Papaleo et al., 2012; Saggu et al., 2013; Jia et al., 2014; Delevoye et al., 2016). We identified a new molecular target sensitive to dysbindin-BLOC-1 defects within the actin cytoskeleton ontology terms, the Arp2/3 complex (Pollard, 2007; Rotty et al., 2013; Spence and Soderling, 2015). This actin regulatory complex was represented by four of seven subunits among our mass spectrometry candidate hits (ACTR3, ARPC1A, ARPC2, and ARPC5). Of these four subunits, we found reduced expression

of ARPC1A, ARPC2, and ACTR3 in Bloc1s5 and 6 shRNA-downregulated cells and confirmed these mass spectrometry results measuring ARPC2 and ARPC5 expression in cells in which BLOC-1 expression was impaired by shRNA or genomic defects. Reduced expression of Arp2/3 complex in BLOC-1 defects has functional consequences, as determined by decreased actin dynamics in early endosomes and suppression of BLOC-1 subunit morphological and plasticity mutant phenotypes by hemideficiencies of Arpc1, a subunit of the *Drosophila* Arp2/3 complex. This BLOC-1 and Arp2/3 pathway is further supported by biochemical interactions of BLOC-1 and Arp2/3 complexes (Fig. 6). Presently, we do not know whether Arp2/3 directly interacts with BLOC-1 or whether BLOC-1 associates with the Arp2/3 complex via either one of three Arp2/3 activators that bind BLOC-1 complex subunits: the WASH complex, WAVE2, or annexin A2 (Ito et al., 2010; Ryder et al., 2013; Delevoye et al., 2016). However, regardless of how BLOC-1, Arp2/3, and an Arp2/3 activator interact, we postulate that BLOC-1 acts upstream of the WASH complex, WAVE2, or annexin A2 to modulate Arp2/3 activity and direct Arp2/3 subcellular localization (Delevoye et al., 2016). In turn, active Arp2/3 would participate in a BLOC-1-actin-dependent endosome sorting event into vesicles or tubules (Ito et al., 2010; Ryder et al., 2013; Delevoye et al., 2016). We favor this model because it explains the following observations presented here and in previous work. First, WASH or annexin A2 downregulation, as well as pharmacological inhibition of Arp2/3, disrupt tubule-dependent BLOC-1 cargo sorting (Ryder et al., 2013; Delevoye et al., 2016). Second, a sequential organization of the BLOC-1, WASH, and Arp2/3 complexes explains that the BLOC-1 complex is unaltered in cells lacking the WASH complex (Fig. 6; Ryder et al., 2013), whereas Arp2/3 subunit expression is reduced in both BLOC-1 and WASH complex mutations (Figs. 5, 6; Ryder et al., 2013). Third, a BLOC-1-activating role upstream of Arp2/3 accounts for the decreased actin dynamics in early endosomes in BLOC-1-deficient cells (Fig. 7). Fourth, sequential organization model of BLOC-1, WASH, and Arp2/3 complexes accounts for the similarity between BLOC-1 and Arp2/3 mutant phenotypes at *Drosophila* synapses. Finally, this model explains the suppression of a synaptic bouton number phenotype in BLOC-1-null alleles by Arp2/3 mutations. At first glance, the suppression of the BLOC-1 bouton phenotype by Arp2/3 alleles could be interpreted as BLOC-1 and Arp2/3 having opposing effects on actin polymerization. However, we do not favor this interpretation because the *Drosophila* synaptic bouton phenotype is a dominant phenotype, which is suppressed by double heterozygotic mutations in two distinct BLOC-1 subunits (Mullin et al., 2015). We interpreted this suppression of the BLOC-1 synaptic phenotype by another BLOC-1 subunit mutant as the removal of BLOC-1 remnants complex with dominant effect (Mullin et al., 2015). Therefore, Arp2/3 deficiencies would suppress a dominant BLOC-1 phenotype, suggesting that the function of BLOC-1 is activating and upstream of the Arp2/3 complex.

Dysbindin, other BLOC-1 subunits, and Arp2/3 complex subunits localize to presynaptic and postsynaptic compartments in neuronal cells (Talbot et al., 2006; Larimore et al., 2013). Dysbindin and BLOC-1 function are presynaptically required for synaptic vesicle protein delivery to and recycling within the nerve terminal and homeostatic synaptic plasticity (Dickman and Davis, 2009; Newell-Litwa et al., 2009; Newell-Litwa et al., 2010; Larimore et al., 2011; Dickman et al., 2012; Di Giovanni and Sheng, 2015; Gokhale et al., 2015b; Mullin et al., 2015). Postsynaptically, dysbindin and Arp2/3 complex subunits are required to modulate spine dynamics, actin polymerization, and neurotransmitter receptor surface expression or total content (Iizuka et al., 2007; Shao et al., 2011; Kim et al., 2013; Rocca et al., 2013; Jia et al., 2014). We used *Drosophila* larvae neurons to address whether presynaptic and dendritic compartments are similarly sensitive to BLOC-1 and Arp2/3 genetic defects. Presynaptic terminals were affected by single-copy loss of either BLOC-1 subunits or Arp2/3 subunits (Figs. 8, 10). However, dendrites were only sensitive to BLOC-1 hemideficiencies, not to a single-copy loss of *Arpc1* (Fig. 9). We postulate two nonexclusive models to explain these results. First, the abundance of Arp2/3 complexes could be limiting in *Drosophila* presynaptic compartments, but not in dendrites, a model drawn from the relative distribution of Arp2/3 complexes in mammalian synapses. Arp2/3 levels are higher in spines compared with axon terminals in mammalian neurons (Rácz and Weinberg, 2008; Korobova and Svitkina, 2010; Spence et al., 2016). A second model considers that Arp2/3 likely interacts with multiple upstream modulators in dendritic compartments, whereas BLOC-1 may be a chief upstream interactor of Arp2/3 complexes in presynaptic terminals. Either model, or combinations of thereof, could account for the lack of effect of a single-copy loss of *Arpc1* in dendritic morphology and the different way by which BLOC-1 and Arp2/3 interact genetically in transheterozygotic analysis in dendrites compared with presynaptic terminals.

Regardless of which one of these models accounts for our observations, both likely converge on a BLOC-1-actin pathway organizing actin-rich domains in organelles. Actin-rich domains in endosomes or synaptic vesicles could participate in protein sorting via endosome tubules or vesicles or to propel vesicles within the synapse (Qualmann et al., 2000). Our finding that *Drosophila* BLOC-1 or Arp2/3 complex hemideficiencies alter the morphology of the *Drosophila* neuromuscular synapse suggest the intriguing possibility that receptors required for maintaining synapse morphology may be sorted from endosomes by BLOC-1-Arp2/3-dependent mechanisms. For example, enhanced TGF-β signaling is sufficient to cause overgrowth of the NMJ, suggesting that disruption of endosome sorting, thus preventing receptor activity downregulation, may contribute to increased synaptic bouton phenotypes (Aberle et al., 2002; Marqués et al., 2002; Harris and Littleton, 2015). This is the case of the late-endosome-localized *spinter*, the mutation of which induces synaptic overgrowth that requires the activity of the TGF-β receptor *wit* (Sweeney and Davis, 2002). If receptor signal transduction is increased in BLOC-1 and Arp2/3 mutant alleles, then synaptic bouton overgrowth should be suppressed in mutants of signal transduction pathways controlling *Drosophila* NMJ morphology (Aberle et al., 2002; Marqués et al., 2002; Harris and Littleton, 2015). Similarly, in mammalian cells, BLOC-1-Arp2/3-dependent mechanisms could control the subcellular localization and activity of other receptor signaling pathways. These include dopamine receptors and NMDA and AMPA glutamatergic receptors, which have been shown previously to be sensitive to BLOC-1 deficiency, as well as other receptors present in the BLOC-1-sensitive proteome such as PLXA2, NRCAM, and cell adhesion molecules (GO: 0005178; Iizuka et al., 2007; Marley and von Zastrow, 2010; Karlsgodt et al., 2011; Shao et al., 2011; Saggu et al., 2013; Orozco et al., 2014).

The unbiased identification of a proteome sensitive to a monogenic defect provides insight into predicting genotype-associated pathways and phenotypes. At a minimum, the BLOC-1-sensitive proteome identifies organelles and subcellular domains in which biogenesis and/or constituents are affected by BLOC-1

deficiencies. The BLOC-1-sensitive proteome predicts effects of BLOC-1 genetic defects on neuronal and non-neuronal organelles. For example, defective melanosome and platelet granule biogenesis characterize BLOC-1 mutations in vertebrates (Raposo and Marks, 2007; Dell'Angelica, 2009; Ghiani and Dell'Angelica, 2011; Wei and Li, 2013). These defective organelles are represented in the GO terms describing pigmentation (GO: 0048753 and GO: 0043473) and platelet granule organization (GO: 0060155) inferred from the BLOC-1-sensitive proteome. Similarly, known functions of the BLOC-1 complex such as interactions with the SNARE membrane fusion machinery or as a factor required for the morphology/composition of presynaptic and postsynaptic domains are encompassed by the SNARE or syntaxin binding (GO: 0000149 and 0017075) and neuron projection morphogenesis (GO: 0048812) ontological categories (Ghiani et al., 2010; Larimore et al., 2011; Dickman et al., 2012; Jia et al., 2014; Di Giovanni and Sheng, 2015; Gokhale et al., 2015b). Our data indicate that the phenotype predictive value of the BLOC-1-sensitive proteome expands to neurodevelopmental disorders such as schizophrenia. The genetic association of polymorphisms in the gene encoding dysbindin (*DTNBP1*) with schizophrenia is disputed (Farrell et al., 2015). However, downregulation of dysbindin expression in brains from schizophrenia patients is a strong argument for dysbindin as a part of the processes associated with disease (Talbot et al., 2004; Tang et al., 2009; Talbot et al., 2011). The BLOC-1-sensitive proteome provides additional insight into the association of dysbindin with schizophrenia because it significantly enriches genes products associated with psychotic disorders as determined with the GDA algorithm (Park et al., 2014). For example, GDA finds 11 gene products in common with the Psychotic Disorders category (F03.700.675) and 31 gene products with the Schizophrenia and Disorders with Psychotic Features category (F03.700; Park et al., 2014). This latter category includes molecules such as the scaffold SHANK1, plexin A2, the enzyme dopamine β hydroxylase. We demonstrated previously that dopamine β hydroxylase coprecipitates with the BLOC-1 complex and the expression of this enzyme is sensitive to BLOC-1 deficiency (Gokhale et al., 2015a). Second, GO analysis of schizophrenia candidate genes identified from genomic or schizophrenia brain gene expression studies overlap with ontology terms inferred from the BLOC-1-sensitive proteome (Gilman et al., 2012; Fromer et al., 2014; Purcell et al., 2014; Föcking et al., 2015; Zhao et al., 2015; Pers et al., 2016). This overlap includes GO terms encompassing actin dynamics, stability, and actin-dependent membrane specializations (Fromer et al., 2014; Zhao et al., 2015). The involvement of actin cytoskeletal components in neurodevelopmental disorders is not just limited to ontologies inferred from candidate genes. In fact, Arp2/3 complex subunit messenger RNAs are reduced in specific layers of the prefrontal cortex of schizophrenia patients (Datta et al., 2016). Moreover, genetic disruption of the neuronal mouse Arp2/3 complex causes schizophrenia endophenotypes (Kim et al., 2015). Genes causative of neurodevelopmental disorders reside upstream of modulators of actin polymerization. Well studied examples are DISC1, which binds kalirin, a protein that activates Rac1 and p21-activated kinase (Hayashi-Takagi et al., 2010; Penzes and Remmers, 2012). SHANK3, a protein that interacts directly with Arp2/3 and the upregulation of which increases filamentous actin in spines (Han et al., 2013). Finally, FMRP binds to CYFIP1 a molecule that regulates the activity of the WAVE1 complex, an Arp2/3 activator, thus establishing a molecular mechanism linking translational control and actin polymerization (Abekhoukh and Bardoni, 2014; Pathania et al., 2014; Yoon et al., 2014). Because dysbindin binds to WAVE2, WAVE-CYFIP-like components in the BLOC-1-sensitive proteome may serve as a platform linking translational control and actin cytoskeleton dynamics. Our work adds significantly to the proposition that Arp2/3-dependent actin polymerization at presynaptic and postsynaptic compartments is a major neurodevelopmental disorder risk pathway. Our results indicate that ontologically prioritized proteomics can offer mechanistic insight into monogenic and polygenic neurodevelopmental disorder pathogenesis, disorder-specific endophenotypes, and genetic modifiers of disease.

References

Abekhoukh S, Bardoni B (2014) CYFIP family proteins between autism and intellectual disability: links with fragile X syndrome. Front Cell Neurosci 8:81. CrossRef Medline

Aberle H, Haghighi AP, Fetter RD, McCabe BD, Magalhães TR, Goodman CS (2002) wishful thinking encodes a BMP type II receptor that regulates synaptic growth in *Drosophila*. Neuron 33:545–558. CrossRef Medline

Albert FW, Treusch S, Shockley AH, Bloom JS, Kruglyak L (2014) Genetics of single-cell protein abundance variation in large yeast populations. Nature 506:494–497. CrossRef Medline

Andersen R, Li Y, Resseguie M, Brenman JE (2005) Calcium/calmodulin-dependent protein kinase II alters structural plasticity and cytoskeletal dynamics in *Drosophila*. J Neurosci 25:8878–8888. CrossRef Medline

Borgesius NZ, van Woerden GM, Buitendijk GH, Keijzer N, Jaarsma D, Hoogenraad CC, Elgersma Y (2011) betaCaMKII plays a nonenzymatic role in hippocampal synaptic plasticity and learning by targeting alpha CaMKII to synapses. J Neurosci 31:10141–10148. CrossRef Medline

Borggrefe T, Wabl M, Akhmedov AT, Jessberger R (1998) A B-cell-specific DNA recombination complex. J Biol Chem 273:17025–17035. CrossRef Medline

Cheli VT, Daniels RW, Godoy R, Hoyle DJ, Kandachar V, Starcevic M, Martinez-Agosto JA, Poole S, DiAntonio A, Lloyd VK, Chang HC, Krantz DE, Dell'Angelica EC (2010) Genetic modifiers of abnormal organelle biogenesis in a *Drosophila* model of BLOC-1 deficiency. Hum Mol Genet 19:861–878. CrossRef Medline

Chen EY, Tan CM, Kou Y, Duan Q, Wang Z, Meirelles GV, Clark NR, Ma'ayan A (2013) Enrichr: interactive and collaborative HTML5 gene list enrichment analysis tool. BMC Bioinformatics 14:128. CrossRef Medline

Ciciotte SL, Gwynn B, Moriyama K, Huizing M, Gahl WA, Bonifacino JS, Peters LL (2003) Cappuccino, a mouse model of Hermansky-Pudlak syndrome, encodes a novel protein that is part of the pallidin-muted complex (BLOC-1). Blood 101:4402–4407. CrossRef Medline

Cox MM, Tucker AM, Tang J, Talbot K, Richer DC, Yeh L, Arnold SE (2009) Neurobehavioral abnormalities in the dysbindin-1 mutant, sandy, on a C57BL/6J genetic background. Genes Brain Behav 8:390–397. CrossRef Medline

Datta D, Arion D, Roman KM, Volk DW, Lewis DA (2016) Altered expression of ARP2/3 complex signaling pathway genes in prefrontal layer 3 pyramidal cells in schizophrenia. Am J Psychiatry. In press. CrossRef Medline

Deibler M, Spatz JP, Kemkemer R (2011) Actin fusion proteins alter the dynamics of mechanically induced cytoskeleton rearrangement. PLoS One 6:e22941. CrossRef Medline

Delevoye C, Heiligenstein X, Ripoll L, Gilles-Marsens F, Dennis MK, Linares RA, Derman L, Gokhale A, Morel E, Faundez V, Marks MS, Raposo G (2016) BLOC-1 brings together the actin and microtubule cytoskeletons to generate recycling endosomes. Curr Biol 26:1–13. CrossRef Medline

Dickman DK, Davis GW (2009) The schizophrenia susceptibility gene dysbindin controls synaptic homeostasis. Science 326:1127–1130. CrossRef Medline

Dickman DK, Tong A, Davis GW (2012) Snapin is critical for presynaptic homeostatic plasticity. J Neurosci 32:8716–8724. CrossRef Medline

Di Giovanni J, Sheng ZH (2015) Regulation of synaptic activity by snapin-mediated endolysosomal transport and sorting. EMBO J 34:2059–2077. CrossRef Medline

Dougherty JD, Schmidt EF, Nakajima M, Heintz N (2010) Analytical approaches to RNA profiling data for the identification of genes enriched in specific cells. Nucl Acids Res 38:4218–4230. CrossRef Medline

Doyle T, Botstein D (1996) Movement of yeast cortical actin cytoskeleton

visualized in vivo. Proc Natl Acad Sci U S A 93:3886–3891. CrossRef Medline

Farrell MS, Werge T, Sklar P, Owen MJ, Ophoff RA, O'Donovan MC, Corvin A, Cichon S, Sullivan PF (2015) Evaluating historical candidate genes for schizophrenia. Mol Psychiatry 20:555–562. CrossRef Medline

Fatjó-Vilas M, Papiol S, Estrada G, Bombín I, Peralta V, Rosa A, Parellada M, Miret S, Martín M, Lázaro L, Campanera S, Muñoz MJ, Lera-Miguel S, Arias B, Navarro ME, Castro-Fornieles J, Cuesta MJ, Arango C, Fañanás L (2011) Dysbindin-1 gene contributes differentially to early- and adult-onset forms of functional psychosis. Am J Med Genet B Neuropsychiatr Genet 156B:322–333. CrossRef Medline

Fei E, Ma X, Zhu C, Xue T, Yan J, Xu Y, Zhou J, Wang G (2010) Nucleocytoplasmic shuttling of dysbindin-1, a schizophrenia-related protein, regulates synapsin I expression. J Biol Chem 285:38630–38640. CrossRef Medline

Ferreira T, Ou Y, Li S, Giniger E, van Meyel DJ (2014) Dendrite architecture organized by transcriptional control of the F-actin nucleator Spire. Development 141:650–660. CrossRef Medline

Föcking M, Lopez LM, English JA, Dicker P, Wolff A, Brindley E, Wynne K, Cagney G, Cotter DR (2015) Proteomic and genomic evidence implicates the postsynaptic density in schizophrenia. Mol Psychiatry 20:424–432. CrossRef Medline

Fontanillo C, Nogales-Cadenas R, Pascual-Montano A, De las Rivas J (2011) Functional analysis beyond enrichment: non-redundant reciprocal linkage of genes and biological terms. PLoS One 6:e24289. CrossRef Medline

Franciscovich AL, Mortimer AD, Freeman AA, Gu J, Sanyal S (2008) Overexpression screen in *Drosophila* identifies neuronal roles of GSK-3 beta/shaggy as a regulator of AP-1-dependent developmental plasticity. Genetics 180:2057–2071. CrossRef Medline

Fromer M et al. (2014) De novo mutations in schizophrenia implicate synaptic networks. Nature 506:179–184. CrossRef Medline

Ghiani CA, Dell'Angelica EC (2011) Dysbindin-containing complexes and their proposed functions in brain: from zero to (too) many in a decade. ASN Neuro 3: pii: e00058. CrossRef Medline

Ghiani CA, Starcevic M, Rodriguez-Fernandez IA, Nazarian R, Cheli VT, Chan LN, Malvar JS, de Vellis J, Sabatti C, Dell'Angelica EC (2009) The dysbindin-containing complex (BLOC-1) in brain: developmental regulation, interaction with SNARE proteins and role in neurite outgrowth. Mol Psychiatry 15:115, 204–215. CrossRef Medline

Gilman SR, Chang J, Xu B, Bawa TS, Gogos JA, Karayiorgou M, Vitkup D (2012) Diverse types of genetic variation converge on functional gene networks involved in schizophrenia. Nat Neurosci 15:1723–1728. CrossRef Medline

Gokhale A, Larimore J, Werner E, So L, Moreno-De-Luca A, Lese-Martin C, Lupashin VV, Smith Y, Faundez V (2012) Quantitative proteomic and genetic analyses of the schizophrenia susceptibility factor dysbindin identify novel roles of the biogenesis of lysosome-related organelles complex 1. J Neurosci 32:3697–3711. CrossRef Medline

Gokhale A, Vrailas-Mortimer A, Larimore J, Comstra HS, Zlatic SA, Werner E, Manvich DF, Iuvone PM, Weinshenker D, Faundez V (2015a) Neuronal copper homeostasis susceptibility by genetic defects in dysbindin, a schizophrenia susceptibility factor. Hum Mol Genet 24:5512–5523. CrossRef Medline

Gokhale A, Mullin AP, Zlatic S, Easley CA 4th, Merritt ME, Raj N, Larimore J, Gordon DE, Peden AA, Sanyal S, Faundez V (2015b) The N-ethylmaleimide sensitive factor (NSF) and dysbindin interact to modulate synaptic plasticity. J Neurosci 35:7643–7653. CrossRef Medline

Gomez TS, Gorman JA, de Narvajas AA, Koenig AO, Billadeau DD (2012) Trafficking defects in WASH-knockout fibroblasts originate from collapsed endosomal and lysosomal networks. Mol Biol Cell 23:3215–3228. CrossRef Medline

Gornick MC, Addington AM, Sporn A, Gogtay N, Greenstein D, Lenane M, Gochman P, Ordonez A, Balkissoon R, Vakkalanka R, Weinberger DR, Rapoport JL, Straub RE (2005) Dysbindin (DTNBP1, 6p22.3) is associated with childhood-onset psychosis and endophenotypes measured by the Premorbid Adjustment Scale (PAS). J Autism Dev Disord 35:831–838. CrossRef Medline

Grueber WB, Ye B, Moore AW, Jan LY, Jan YN (2003) Dendrites of distinct classes of *Drosophila* sensory neurons show different capacities for homotypic repulsion. Curr Biol 13:618–626. CrossRef Medline

Gulsuner S, Walsh T, Watts AC, Lee MK, Thornton AM, Casadei S, Rippey C, Shahin H; Consortium on the Genetics of Schizophrenia (COGS); PAARTNERS Study Group, Nimgaonkar VL, Go RC, Savage RM, Swerdlow NR, Gur RE, Braff DL, King MC, McClellan JM (2013) Spatial and temporal mapping of de novo mutations in schizophrenia to a fetal prefrontal cortical network. Cell 154:518–529. CrossRef Medline

Gwynn B, Martina JA, Bonifacino JS, Sviderskaya EV, Lamoreux ML, Bennett DC, Moriyama K, Huizing M, Helip-Wooley A, Gahl WA, Webb LS, Lambert AJ, Peters LL (2004) Reduced pigmentation (rp), a mouse model of Hermansky-Pudlak syndrome, encodes a novel component of the BLOC-1 complex. Blood 104:3181–3189. CrossRef Medline

Han K, Holder JL Jr, Schaaf CP, Lu H, Chen H, Kang H, Tang J, Wu Z, Hao S, Cheung SW, Yu P, Sun H, Breman AM, Patel A, Lu HC, Zoghbi HY (2013) SHANK3 overexpression causes manic-like behaviour with unique pharmacogenetic properties. Nature 503:72–77. CrossRef Medline

Harris KP, Littleton JT (2015) Transmission, development, and plasticity of synapses. Genetics 201:345–375. CrossRef Medline

Hayashi-Takagi A, Takaki M, Graziane N, Seshadri S, Murdoch H, Dunlop AJ, Makino Y, Seshadri AJ, Ishizuka K, Srivastava DP, Xie Z, Baraban JM, Houslay MD, Tomoda T, Brandon NJ, Kamiya A, Yan Z, Penzes P, Sawa A (2010) Disrupted-in-Schizophrenia 1 (DISC1) regulates spines of the glutamate synapse via Rac1. Nat Neurosci 13:327–332. CrossRef Medline

Huang Da W, Sherman BT, Lempicki RA (2009) Systematic and integrative analysis of large gene lists using DAVID bioinformatics resources. Nat Protoc 4:44–57. CrossRef Medline

Huang L, Kuo YM, Gitschier J (1999) The pallid gene encodes a novel, syntaxin 13-interacting protein involved in platelet storage pool deficiency. Nat Genet 23:329–332. CrossRef Medline

Hudson AM, Cooley L (2002) A subset of dynamic actin rearrangements in *Drosophila* requires the Arp2/3 complex. J Cell Biol 156:677–687. CrossRef Medline

Ihara S, Oka T, Fukui Y (2006) Direct binding of SWAP-70 to non-muscle actin is required for membrane ruffling. J Cell Sci 119:500–507. CrossRef Medline

Iizuka Y, Sei Y, Weinberger DR, Straub RE (2007) Evidence that the BLOC-1 protein dysbindin modulates dopamine D2 receptor internalization and signaling but not D1 internalization. J Neurosci 27:12390–12395. CrossRef Medline

Ito H, Morishita R, Shinoda T, Iwamoto I, Sudo K, Okamoto K, Nagata K (2010) Dysbindin-1, WAVE2 and Abi-1 form a complex that regulates dendritic spine formation. Mol Psychiatry 15:976–986. CrossRef Medline

Iyer EP, Iyer SC, Sullivan L, Wang D, Meduri R, Graybeal LL, Cox DN (2013a) Functional genomic analyses of two morphologically distinct classes of *Drosophila* sensory neurons: post-mitotic roles of transcription factors in dendritic patterning. PLoS One 8:e72434. CrossRef Medline

Iyer SC, Wang D, Iyer EP, Trunnell SA, Meduri R, Shinwari R, Sulkowski MJ, Cox DN (2012) The RhoGEF trio functions in sculpting class specific dendrite morphogenesis in *Drosophila* sensory neurons. PLoS One 7:e33634. CrossRef Medline

Iyer SC, Ramachandran Iyer EP, Meduri R, Rubaharan M, Kuntimaddi A, Karamsetty M, Cox DN (2013b) Cut, via CrebA, transcriptionally regulates the COPII secretory pathway to direct dendrite development in *Drosophila*. J Cell Sci 126:4732–4745. CrossRef Medline

Jentsch JD, Trantham-Davidson H, Jairl C, Tinsley M, Cannon TD, Lavin A (2009) Dysbindin modulates prefrontal cortical glutamatergic circuits and working memory function in mice. Neuropsychopharmacology 34:2601–2608. CrossRef Medline

Jia JM, Hu Z, Nordman J, Li Z (2014) The schizophrenia susceptibility gene dysbindin regulates dendritic spine dynamics. J Neurosci 34:13725–13736. CrossRef Medline

Jinushi-Nakao S, Arvind R, Amikura R, Kinameri E, Liu AW, Moore AW (2007) Knot/Collier and cut control different aspects of dendrite cytoskeleton and synergize to define final arbor shape. Neuron 56:963–978. CrossRef Medline

Karlsgodt KH, Robleto K, Trantham-Davidson H, Jairl C, Cannon TD, Lavin A, Jentsch JD (2011) Reduced dysbindin expression mediates N-methyl-D-aspartate receptor hypofunction and impaired working memory performance. Biol Psychiatry 69:28–34. CrossRef Medline

Kim IH, Rácz B, Wang H, Burianek L, Weinberg R, Yasuda R, Wetsel WC, Soderling SH (2013) Disruption of Arp2/3 results in asymmetric structural plasticity of dendritic spines and progressive synaptic and behavioral abnormalities. J Neurosci 33:6081–6092. CrossRef Medline

Kim IH, Rossi MA, Aryal DK, Rácz B, Kim N, Uezu A, Wang F, Wetsel WC, Weinberg RJ, Yin H, Soderling SH (2015) Spine pruning drives

antipsychotic-sensitive locomotion via circuit control of striatal dopamine. Nat Neurosci 18:883–891. CrossRef Medline

Korobova F, Svitkina T (2010) Molecular architecture of synaptic actin cytoskeleton in hippocampal neurons reveals a mechanism of dendritic spine morphogenesis. Mol Biol Cell 21:165–176. CrossRef Medline

Kushimoto T, Basrur V, Valencia J, Matsunaga J, Vieira WD, Ferrans VJ, Muller J, Appella E, Hearing VJ (2001) A model for melanosome biogenesis based on the purification and analysis of early melanosomes. Proc Natl Acad Sci U S A 98:10698–10703. CrossRef Medline

Larimore J, Tornieri K, Ryder PV, Gokhale A, Zlatic SA, Craige B, Lee JD, Talbot K, Pare JF, Smith Y, Faundez V (2011) The schizophrenia susceptibility factor dysbindin and its associated complex sort cargoes from cell bodies to the synapse. Mol Biol Cell 22:4854–4867. CrossRef Medline

Larimore J, Ryder PV, Kim KY, Ambrose LA, Chapleau C, Calfa G, Gross C, Bassell GJ, Pozzo-Miller L, Smith Y, Talbot K, Park IH, Faundez V (2013) MeCP2 regulates the synaptic expression of a Dysbindin-BLOC-1 network component in mouse brain and human induced pluripotent stem cell-derived neurons. PLoS One 8:e65069. CrossRef Medline

Larimore J, Zlatic SA, Gokhale A, Tornieri K, Singleton KS, Mullin AP, Tang J, Talbot K, Faundez V (2014) Mutations in the BLOC-1 subunits dysbindin and muted generate divergent and dosage-dependent phenotypes. J Biol Chem 289:14291–14300. CrossRef Medline

Li W, Zhang Q, Oiso N, Novak EK, Gautam R, O'Brien EP, Tinsley CL, Blake DJ, Spritz RA, Copeland NG, Jenkins NA, Amato D, Roe BA, Starcevic M, Dell'Angelica EC, Elliott RW, Mishra V, Kingsmore SF, Paylor RE, Swank RT (2003) Hermansky-Pudlak syndrome type 7 (HPS-7) results from mutant dysbindin, a member of the biogenesis of lysosome-related organelles complex 1 (BLOC-1). Nat Genet 35:84–89. CrossRef Medline

Lim C, Allada R (2013) ATAXIN-2 activates PERIOD translation to sustain circadian rhythms in *Drosophila*. Science 340:875–879. CrossRef Medline

Marley A, von Zastrow M (2010) Dysbindin promotes the post-endocytic sorting of G protein-coupled receptors to lysosomes. PLoS One 5:e9325. CrossRef Medline

Marqués G, Bao H, Haerry TE, Shimell MJ, Duchek P, Zhang B, O'Connor MB (2002) The *Drosophila* BMP type II receptor Wishful Thinking regulates neuromuscular synapse morphology and function. Neuron 33:529–543. CrossRef Medline

Merico D, Isserlin R, Stueker O, Emili A, Bader GD (2010) Enrichment map: a network-based method for gene-set enrichment visualization and interpretation. PLoS One 5:e13984. CrossRef Medline

Morel E, Parton RG, Gruenberg J (2009) Annexin A2-dependent polymerization of actin mediates endosome biogenesis. Dev Cell 16:445–457. CrossRef Medline

Mullin AP, Gokhale A, Larimore J, Faundez V (2011) Cell biology of the BLOC-1 complex subunit dysbindin, a schizophrenia susceptibility gene. Mol Neurobiol 44:53–64. CrossRef Medline

Mullin AP, Gokhale A, Moreno-De-Luca A, Sanyal S, Waddington JL, Faundez V (2013) Neurodevelopmental disorders: mechanisms and boundary definitions from genomes, interactomes and proteomes. Transl Psychiatry 3:e329. CrossRef Medline

Mullin AP, Sadanandappa MK, Ma W, Dickman DK, VijayRaghavan K, Ramaswami M, Sanyal S, Faundez V (2015) Gene dosage in the dysbindin schizophrenia susceptibility network differentially affect synaptic function and plasticity. J Neurosci 35:325–338. CrossRef Medline

Nagy A, Delgado-Escueta AV (1984) Rapid preparation of synaptosomes from mammalian brain using nontoxic isoosmotic gradient material (Percoll). J Neurochem 43:1114–1123. CrossRef Medline

Network and Pathway Analysis Subgroup of Psychiatric Genomics Consortium (2015) Psychiatric genome-wide association study analyses implicate neuronal, immune and histone pathways. Nat Neurosci 18:199–209. CrossRef Medline

Newell-Litwa K, Salazar G, Smith Y, Faundez V (2009) Roles of BLOC-1 and adaptor protein-3 complexes in cargo sorting to synaptic vesicles. Mol Biol Cell 20:1441–1453. CrossRef Medline

Newell-Litwa K, Chintala S, Jenkins S, Pare JF, McGaha L, Smith Y, Faundez V (2010) Hermansky-Pudlak protein complexes, AP-3 and BLOC-1, differentially regulate presynaptic composition in the striatum and hippocampus. J Neurosci 30:820–831. CrossRef Medline

Numakawa T, Yagasaki Y, Ishimoto T, Okada T, Suzuki T, Iwata N, Ozaki N, Taguchi T, Tatsumi M, Kamijima K, Straub RE, Weinberger DR, Kunugi H, Hashimoto R (2004) Evidence of novel neuronal functions of dysbindin, a susceptibility gene for schizophrenia. Hum Mol Genet 13:2699–2708. CrossRef Medline

Okada N et al. (2016) Abnormal asymmetries in subcortical brain volume in schizophrenia. Mol Psychiatry 21:1460–1466. CrossRef Medline

Ong SE, Blagoev B, Kratchmarova I, Kristensen DB, Steen H, Pandey A, Mann M (2002) Stable isotope labeling by amino acids in cell culture, SILAC, as a simple and accurate approach to expression proteomics. Mol Cell Proteomics 1:376–386. CrossRef Medline

Orozco IJ, Koppensteiner P, Ninan I, Arancio O (2014) The schizophrenia susceptibility gene DTNBP1 modulates AMPAR synaptic transmission and plasticity in the hippocampus of juvenile DBA/2J mice. Mol Cell Neurosci 58:76–84. CrossRef Medline

Papaleo F, Yang F, Garcia S, Chen J, Lu B, Crawley JN, Weinberger DR (2012) Dysbindin-1 modulates prefrontal cortical activity and schizophrenia-like behaviors via dopamine/D2 pathways. Mol Psychiatry 17:85–98. CrossRef Medline

Park J, Wick HC, Kee DE, Noto K, Maron JL, Slonim DK (2014) Finding novel molecular connections between developmental processes and disease. PLoS Comput Biol 10:e1003578. CrossRef Medline

Parks AL et al. (2004) Systematic generation of high-resolution deletion coverage of the *Drosophila* melanogaster genome. Nat Genet 36:288–292. CrossRef Medline

Pathania M, Davenport EC, Muir J, Sheehan DF, López-Doménech G, Kittler JT (2014) The autism and schizophrenia associated gene CYFIP1 is critical for the maintenance of dendritic complexity and the stabilization of mature spines. Transl Psychiatry 4:e374. CrossRef Medline

Penzes P, Remmers C (2012) Kalirin signaling: implications for synaptic pathology. Mol Neurobiol 45:109–118. CrossRef Medline

Perez-Cornejo P, Gokhale A, Duran C, Cui Y, Xiao Q, Hartzell HC, Faundez V (2012) Anoctamin 1 (Tmem16A) Ca2+-activated chloride channel stoichiometrically interacts with an ezrin-radixin-moesin network. Proc Natl Acad Sci U S A 109:10376–10381. CrossRef Medline

Pers TH, Timshel P, Ripke S, Lent S, Sullivan PF, O'Donovan MC, Franke L, Hirschhorn JN; Schizophrenia Working Group of the Psychiatric Genomics Consortium (2016) Comprehensive analysis of schizophrenia-associated loci highlights ion channel pathways and biologically plausible candidate causal genes. Hum Mol Genet 25:1247–1254. CrossRef Medline

Picotti P, Clément-Ziza M, Lam H, Campbell DS, Schmidt A, Deutsch EW, Röst H, Sun Z, Rinner O, Reiter L, Shen Q, Michaelson JJ, Frei A, Alberti S, Kusebauch U, Wollscheid B, Moritz RL, Beyer A, Aebersold R (2013) A complete mass-spectrometric map of the yeast proteome applied to quantitative trait analysis. Nature 494:266–270. CrossRef Medline

Pollard TD (2007) Regulation of actin filament assembly by Arp2/3 complex and formins. Annu Rev Biophys Biomol Struct 36:451–477. CrossRef Medline

Pollard TD, Hanein D, Volkmann N (2002) Arp2/3 plays no role in muscle contraction. Nature 418:915. Medline

Purcell SM et al. (2014) A polygenic burden of rare disruptive mutations in schizophrenia. Nature 506:185–190. CrossRef Medline

Puthenveedu MA, Lauffer B, Temkin P, Vistein R, Carlton P, Thorn K, Taunton J, Weiner OD, Parton RG, von Zastrow M (2010) Sequence-dependent sorting of recycling proteins by actin-stabilized endosomal microdomains. Cell 143:761–773. CrossRef Medline

Qualmann B, Kessels MM, Kelly RB (2000) Molecular links between endocytosis and the actin cytoskeleton. J Cell Biol 150:F111–116. CrossRef Medline

Rácz B, Weinberg RJ (2008) Organization of the Arp2/3 complex in hippocampal spines. J Neurosci 28:5654–5659. CrossRef Medline

Raposo G, Marks MS (2007) Melanosomes–dark organelles enlighten endosomal membrane transport. Nat Rev Mol Cell Biol 8:786–797. CrossRef Medline

Riedl J, Crevenna AH, Kessenbrock K, Yu JH, Neukirchen D, Bista M, Bradke F, Jenne D, Holak TA, Werb Z, Sixt M, Wedlich-Soldner R (2008) Lifeact: a versatile marker to visualize F-actin. Nat Methods 5:605–607. CrossRef Medline

Rocca DL, Amici M, Antoniou A, Blanco Suarez E, Halemani N, Murk K, McGarvey J, Jaafari N, Mellor JR, Collingridge GL, Hanley JG (2013) The small GTPase Arf1 modulates Arp2/3-mediated actin polymerization via PICK1 to regulate synaptic plasticity. Neuron 79:293–307. CrossRef Medline

Rotty JD, Wu C, Bear JE (2013) New insights into the regulation and cellular

functions of the ARP2/3 complex. Nat Rev Mol Cell Biol 14:7–12. CrossRef Medline

Ruepp A, Waegele B, Lechner M, Brauner B, Dunger-Kaltenbach I, Fobo G, Frishman G, Montrone C, Mewes HW (2010) CORUM: the comprehensive resource of mammalian protein complexes–2009. Nucl Acids Res 38:D497–501. CrossRef Medline

Ryder PV, Vistein R, Gokhale A, Seaman MN, Puthenveedu MA, Faundez V (2013) The WASH complex, an endosomal Arp2/3 activator, interacts with the Hermansky-Pudlak syndrome complex BLOC-1 and its cargo phosphatidylinositol-4-kinase type II alpha. Mol Biol Cell 24:2269–2284. CrossRef Medline

Saggu S, Cannon TD, Jentsch JD, Lavin A (2013) Potential molecular mechanisms for decreased synaptic glutamate release in dysbindin-1 mutant mice. Schizophr Res 146:254–263. CrossRef Medline

Salazar G, Craige B, Styers ML, Newell-Litwa KA, Doucette MM, Wainer BH, Falcon-Perez JM, Dell'Angelica EC, Peden AA, Werner E, Faundez V (2006) BLOC-1 complex deficiency alters the targeting of adaptor protein complex-3 cargoes. Mol Biol Cell 17:4014–4026. CrossRef Medline

Seaman MN, Gautreau A, Billadeau DD (2013) Retromer-mediated endosomal protein sorting: all WASHed up! Trends Cell Biol 23:522–528. CrossRef Medline

Setty SR, Tenza D, Truschel ST, Chou E, Sviderskaya EV, Theos AC, Lamoreux ML, Di Pietro SM, Starcevic M, Bennett DC, Dell'Angelica EC, Raposo G, Marks MS (2007) BLOC-1 is required for cargo-specific sorting from vacuolar early endosomes toward lysosome-related organelles. Mol Biol Cell 18:768–780. CrossRef Medline

Setty SR, Tenza D, Sviderskaya EV, Bennett DC, Raposo G, Marks MS (2008) Cell-specific ATP7A transport sustains copper-dependent tyrosinase activity in melanosomes. Nature 454:1142–1146. CrossRef Medline

Shannon P, Markiel A, Ozier O, Baliga NS, Wang JT, Ramage D, Amin N, Schwikowski B, Ideker T (2003) Cytoscape: a software environment for integrated models of biomolecular interaction networks. Genome Res 13:2498–2504. CrossRef Medline

Shao L, Shuai Y, Wang J, Feng S, Lu B, Li Z, Zhao Y, Wang L, Zhong Y (2011) Schizophrenia susceptibility gene dysbindin regulates glutamatergic and dopaminergic functions via distinctive mechanisms in *Drosophila*. Proc Natl Acad Sci U S A 108:18831–18836. CrossRef Medline

Shimono K, Fujishima K, Nomura T, Ohashi M, Usui T, Kengaku M, Toyoda A, Uemura T (2014) An evolutionarily conserved protein CHORD regulates scaling of dendritic arbors with body size. Sci Rep 4:4415. CrossRef Medline

Shinohara M, Terada Y, Iwamatsu A, Shinohara A, Mochizuki N, Higuchi M, Gotoh Y, Ihara S, Nagata S, Itoh H, Fukui Y, Jessberger R (2002) SWAP-70 is a guanine-nucleotide-exchange factor that mediates signalling of membrane ruffling. Nature 416:759–763. CrossRef Medline

Spence EF, Soderling SH (2015) Actin out: regulation of the synaptic cytoskeleton. J Biol Chem 290:28613–28622. CrossRef Medline

Spence EF, Kanak DJ, Carlson BR, Soderling SH (2016) The Arp2/3 complex is essential for distinct stages of spine synapse maturation, including synapse unsilencing. J Neurosci 36:9696–9709. CrossRef Medline

Starcevic M, Dell'Angelica EC (2004) Identification of snapin and three novel proteins (BLOS1, BLOS2, and BLOS3/reduced pigmentation) as subunits of biogenesis of lysosome-related organelles complex-1 (BLOC-1). J Biol Chem 279:28393–28401. CrossRef Medline

Straub RE, Jiang Y, MacLean CJ, Ma Y, Webb BT, Myakishev MV, Harris-Kerr C, Wormley B, Sadek H, Kadambi B, Cesare AJ, Gibberman A, Wang X, O'Neill FA, Walsh D, Kendler KS (2002) Genetic variation in the 6p22.3 gene DTNBP1, the human ortholog of the mouse dysbindin gene, is associated with schizophrenia. Am J Hum Genet 71:337–348. CrossRef Medline

Sulkowski MJ, Iyer SC, Kurosawa MS, Iyer EP, Cox DN (2011) Turtle functions downstream of Cut in differentially regulating class specific dendrite morphogenesis in *Drosophila*. PLoS One 6:e22611. CrossRef Medline

Suto F, Tsuboi M, Kamiya H, Mizuno H, Kiyama Y, Komai S, Shimizu M, Sanbo M, Yagi T, Hiromi Y, Chédotal A, Mitchell KJ, Manabe T, Fujisawa H (2007) Interactions between plexin-A2, plexin-A4, and semaphorin 6A control lamina-restricted projection of hippocampal mossy fibers. Neuron 53:535–547. CrossRef Medline

Sweeney ST, Davis GW (2002) Unrestricted synaptic growth in spinster-a late endosomal protein implicated in TGF-beta-mediated synaptic growth regulation. Neuron 36:403–416. CrossRef Medline

Talbot K, Eidem WL, Tinsley CL, Benson MA, Thompson EW, Smith RJ, Hahn CG, Siegel SJ, Trojanowski JQ, Gur RE, Blake DJ, Arnold SE (2004) Dysbindin-1 is reduced in intrinsic, glutamatergic terminals of the hippocampal formation in schizophrenia. J Clin Invest 113:1353–1363. CrossRef Medline

Talbot K, Cho DS, Ong WY, Benson MA, Han LY, Kazi HA, Kamins J, Hahn CG, Blake DJ, Arnold SE (2006) Dysbindin-1 is a synaptic and microtubular protein that binds brain snapin. Hum Mol Genet 15:3041–3054. CrossRef Medline

Talbot K, Ong WY, Blake DJ, Tang D, Louneva N, Carlson GC, Arnold SE (2009) Dysbindin-1 and its protein family, with special attention to the potential role of dysbindin-1 in neuronal functions and the pathophysiology of schizophrenia. In: Handbook of neurochemistry and molecular neurobiology (Kantrowitz J, ed), pp 107–241. New York: Springer Science.

Talbot K, Louneva N, Cohen JW, Kazi H, Blake DJ, Arnold SE (2011) Synaptic dysbindin-1 reductions in schizophrenia occur in an isoform-specific manner indicating their subsynaptic location. PLoS One 6:e16886. CrossRef Medline

Tang J, LeGros RP, Louneva N, Yeh L, Cohen JW, Hahn CG, Blake DJ, Arnold SE, Talbot K (2009) Dysbindin-1 in dorsolateral prefrontal cortex of schizophrenia cases is reduced in an isoform-specific manner unrelated to dysbindin-1 mRNA expression. Hum Mol Genet 18:3851–3863. CrossRef Medline

Thompson A, Schäfer J, Kuhn K, Kienle S, Schwarz J, Schmidt G, Neumann T, Johnstone R, Mohammed AK, Hamon C (2003) Tandem mass tags: a novel quantification strategy for comparative analysis of complex protein mixtures by MS/MS. Anal Chem 75:1895–1904. CrossRef Medline

van Erp TG et al. (2016) Subcortical brain volume abnormalities in 2028 individuals with schizophrenia and 2540 healthy controls via the ENIGMA consortium. Mol Psychiatry 21:547–553. CrossRef Medline

Wei AH, Li W (2013) Hermansky-Pudlak syndrome: pigmentary and non-pigmentary defects and their pathogenesis. Pigment Cell Melanoma Res 26:176–192. CrossRef Medline

Wei ML (2006) Hermansky-Pudlak syndrome: a disease of protein trafficking and organelle function. Pigment Cell Res 19:19–42. CrossRef Medline

Wolf C, Jackson MC, Kissling C, Thome J, Linden DE (2011) Dysbindin-1 genotype effects on emotional working memory. Mol Psychiatry 16:145–155. CrossRef Medline

Wu L, Candille SI, Choi Y, Xie D, Jiang L, Li-Pook-Than J, Tang H, Snyder M (2013) Variation and genetic control of protein abundance in humans. Nature 499:79–82. CrossRef Medline

Yang Q, He X, Yang L, Zhou Z, Cullinane AR, Wei A, Zhang Z, Hao Z, Zhang A, He M, Feng Y, Gao X, Gahl WA, Huizing M, Li W (2012) The BLOS1-interacting protein KXD1 is involved in the biogenesis of lysosome-related organelles. Traffic 13:1160–1169. CrossRef Medline

Yokoshi M, Li Q, Yamamoto M, Okada H, Suzuki Y, Kawahara Y (2014) Direct binding of Ataxin-2 to distinct elements in 3′ UTRs promotes mRNA stability and protein expression. Mol Cell 55:186–198. CrossRef Medline

Yoon KJ et al. (2014) Modeling a genetic risk for schizophrenia in iPSCs and mice reveals neural stem cell deficits associated with adherens junctions and polarity. Cell Stem Cell 15:79–91. CrossRef Medline

Zhang Q, Li W, Novak EK, Karim A, Mishra VS, Kingsmore SF, Roe BA, Suzuki T, Swank RT (2002) The gene for the muted (mu) mouse, a model for Hermansky-Pudlak syndrome, defines a novel protein which regulates vesicle trafficking. Hum Mol Genet 11:697–706. CrossRef Medline

Zhao Z, Xu J, Chen J, Kim S, Reimers M, Bacanu SA, Yu H, Liu C, Sun J, Wang Q, Jia P, Xu F, Zhang Y, Kendler KS, Peng Z, Chen X (2015) Transcriptome sequencing and genome-wide association analyses reveal lysosomal function and actin cytoskeleton remodeling in schizophrenia and bipolar disorder. Mol Psychiatry 20:563–572. CrossRef Medline